TURUN YLIOPISTON JULKAISUJA
ANNALES UNIVERSITATIS TURKUENSIS

SARJA - SER. D OSA - TOM. 941

MEDICA - ODONTOLOGICA

STRUCTURAL STUDIES ON ENZYMES OF BIOTECHNOLOGICAL AND BIOMEDICAL INTEREST

by

Prathusha Dhavala

TURUN YLIOPISTO
UNIVERSITY OF TURKU
Turku 2010

From
Turku Centre for Biotechnology, University of Turku and Åbo Akademi University;
Department of Biochemistry and Food Chemistry, University of Turku

Supervised by
Docent Anastassios C. Papageorgiou, Ph.D
Turku Centre for Biotechnology
University of Turku and Åbo Akademi University
Turku, Finland

Reviewed by
Assoc. Professor Ester Boix, Ph.D
Departament de Bioquímica i Biologia Molecular
Facultat de Biociéncies
Universitat Autònoma de Barcelona
Barcelona, Spain

Docent Petri Kursula, Ph.D
Department of Biochemistry
University of Oulu
Oulu, Finland

Opponent
Professor Inger Andersson, Ph.D
Department of Molecular Biology
Uppsala University
Uppsala, Sweden

ISBN 978-951-29-4489-7 (PRINT)
ISBN 978-951-29-4490-3 (PDF)
ISSN 0355-9483
Painosalama Oy – Turku, Finland 2011

"Om sahanaa vavatu sahanau bhunaktu
saha veeryam karavaavahai
tejasvi naavadheetamastu maa vidvishaavahai
Om shantih shantih shantih"
Om ! May He protect us both together; may He nourish us both together;
May we work conjointly with great energy,
May our study be vigorous and effective;
May we not mutually dispute,
Om ! Let there be Peace in me,
Let there be Peace in my environment,
Let there be Peace in the forces that act on me

- Taittiriya Upanishad

"na hi jnanena sadrsam pavitram iha vidyate"
In this world, there is nothing as sublime and pure as transcendental knowledge

- Bhagavad Gita

TABLE OF CONTENTS

LIST OF ORIGINAL PUBLICATIONS

This thesis is based on the following articles that are referred to in the text by their Roman numerals.

I Dhavala P, Krasotkina J, Dubreuil C, Papageorgiou AC (2008). Expression, purification and crystallization of *Helicobacter pylori* L-asparaginase. *Acta Cryst.* **F64**, 740-742.

II Axarli I, Dhavala P, Papageorgiou AC, Labrou NE (2009). Crystallographic and functional characterization of the fluorodifen-inducible glutathione transferase from *Glycine max* reveals an active site topography suited for diphenylether herbicides and a novel L-site. *J. Mol. Biol.* **385**, 984-1002.

III Axarli I, Dhavala P, Papageorgiou AC, Labrou NE (2009). Crystal structure of *Glycine max* glutathione transferase in complex with glutathione: investigation of the mechanism operating by the Tau class glutathione transferases. *Biochem. J.* **422**, 247-56.

IV Dhavala P, Papageorgiou AC (2009). Structure of *Helicobacter pylori* L-asparaginase at 1.4 Å resolution. *Acta Cryst.* **D65**, 1253-61.

ABSTRACT

Structural studies of proteins aim at elucidating the atomic details of molecular interactions in biological processes of living organisms. These studies are particularly important in understanding structure, function and evolution of proteins and in defining their roles in complex biological settings. Furthermore, structural studies can be used for the development of novel properties in biomolecules of environmental, industrial and medical importance. X-ray crystallography is an invaluable tool to obtain accurate and precise information about the structure of proteins at the atomic level.

Glutathione transferases (GSTs) are amongst the most versatile enzymes in nature. They are able to catalyze a wide variety of conjugation reactions between glutathione (GSH) and non-polar components containing an electrophilic carbon, nitrogen or sulphur atom. Plant GSTs from the Tau class (a poorly characterized class) play an important role in the detoxification of xenobiotics and stress tolerance. Structural studies were performed on a Tau class fluorodifen-inducible glutathione transferase from *Glycine max* (GmGSTU4-4) complexed with GSH (2.7 Å) and a product analogue Nb-GSH (1.7 Å). The three-dimensional structure of the GmGSTU4-4-GSH complex revealed that GSH binds in different conformations in the two subunits of the dimer: in an ionized form in one subunit and a non-ionized form in the second subunit. Only the ionized form of the substrate may lead to the formation of a catalytically competent complex. Structural comparison between the GSH and Nb-GSH bound complexes revealed significant differences with respect to the hydrogen-bonding, electrostatic interaction pattern, the upper part of α-helix H4 and the C-terminus of the enzyme. These differences indicate an intrasubunit modulation between the G-and H-sites suggesting an induced-fit mechanism of xenobiotic substrate binding. A novel binding site on the surface of the enzyme was also revealed.

Bacterial type-II L-asparaginases are used in the treatment of haematopoietic diseases such as acute lymphoblastic leukaemia (ALL) and lymphomas due to their ability to catalyze the conversion of L-asparagine to L-aspartate and ammonia. *Escherichia coli* and *Erwinia chrysanthemi* asparaginases are employed for the treatment of ALL for over 30 years. However, serious side-effects affecting the liver and pancreas have been observed due to the intrinsic glutaminase activity of the administered enzymes. Structural studies on *Helicobacter pylori* L-asparaginase (HpA) were carried out in an effort to discover novel L-asparaginases with potential chemotherapeutic utility in ALL treatment. Detailed analysis of the active site geometry revealed structurally significant differences between HpA and other L-asparaginases that may be important for the biological activities of the enzyme and could be further exploited in protein engineering efforts.

ABBREVIATIONS

ALL	acute lymphoblastic leukaemia
ASK1	apoptosis signal-regulating kinase
ATP	adenosine-5´-triphosphate
CDNB	1-chloro-2, 4-dinitrobenzene
cGST	cytoplasmic glutathione S-transferases
DHAR	dehyrdroascorbate reductases
EcAII	*Escherichia coli* periplasmic L-asparaginase
EwA	*Erwinia carotovora* L-asparaginase
ErA	*Erwinia chrysanthemi* L-asparaginase
γ-ECS	γ-glutamyl-cysteine-synthetase
γ-EC	γ-glutamyl-cysteine
GFP	green fluorescent protein
GSH	reduced glutathione
GST	glutathione transferase (formerly known as glutathione S-transferase)
GSTO	Omega class of GST
GSTP	Pi class of GST
GT	glucosyltransferase
GTX	S-hexylglutathione
GmGSTU4-4	*Glycine max* GST Tau 4-4
G-site	GSH-binding site
HpA	*Helicobacter pylori* L-asparaginase
hGSTA1-1	human GST Alpha 1-1
H-site	hydrophobic binding site
MAPEG	membrane-associated proteins involved in eicosanoid and glutathione metabolism
Nb-GSH	S-(p-nitrobenzyl)-glutathione
NpM	(4-nitrophenyl) methanethiol
PEG	polyethylene glycol
PEG-ASP	pegylated L-asparaginase
PgA	*Pseudomonas* 7A glutaminase L-asparaginase
RMSD	root mean square deviation
TCHQD	tetrachlorohydroquinone dehalogenase
TRX	thioredoxin-like fold
TLK286	canfosfamide hydrochloride
WsA	*Wolinella succinogenes* L-asparaginase

1 LITERATURE REVIEW

1.1 Glutathione transferase superfamily

The discovery of the catalytic activity of an enzyme responsible for the conjugation of glutathione (GSH) to 1,2-dichloro-4-nitrobenzene in the cytosolic extracts of rat liver occurred in the year 1961 [1]. The enzyme was later identified as glutathione S-transferase (GST; E.C. 2.5.1.18). This led to an increasing interest in the genetics, enzymology and structural studies of GSTs and their role in conjugation reactions. The existence of GSTs in plants was first discovered in the early 1970s when a GST from maize was shown to be responsible for the conjugation of chloro-S-triazine atrizine with GSH, thereby protecting the crop from the herbicide [2]. Since then, the identification of the activities of GSTs or their corresponding enzymes/gene sequences in animals, plants and fungi has taken place [3, 4]. Furthermore, the structural information of the GSTs has had a profound impact on our understanding of their catalytic mechanism, protein fold evolution, and the molecular basis of detoxification of endogenous and xenobiotic electrophiles. Issues such as the recognition and the activation of glutathione for nucleophilic attack and the specific recognition of the electrophilic substrates by the enzyme have been well explained with the help of structural studies [5].

1.1.1 Importance of detoxification

All living organisms are constantly exposed to non-nutritional foreign chemical species commonly known as xenobiotics. Xenobiotics are potentially toxic to the organisms because they possess electrophilic centres that could readily form covalent bonds with the nucleophilic centres of proteins and nucleic acids and intervene with the metabolic processes. Most xenobiotics are naturally occurring compounds of microbial, animal and plant origin. Furthermore, a range of novel human-made chemicals such as agrichemicals (herbicides and pesticides) and industrial by-products that contaminate the ground water and soil pose a serious threat to the environment and to organisms.

Plants, in particular, are subjected to greater xenobiotic challenges owing to their direct contact with the contaminants. Hence, they have to develop more efficient ways of xenobiotic detoxification for their survival. As a result, the plant mechanisms in response to the xenobiotic compounds are of great importance to the natural world, agriculture, and human health and could provide a more reliable, natural, and inexpensive method of environmental cleansing. GSTs are the enzymes which play a major role in xenobiotic detoxification process [6, 7].

1.1.1.1 The detoxification process

The whole detoxification process can be subdivided into three phases (Fig. 1) [8, 9]:

- Phase I (activation): The initial phase of chemical activation of the xenobiotic compound is achieved mostly by hydrolysis, oxidation or reduction reactions

catalyzed by esterases (P-450 monooxygenases and peroxidases) [10, 11]. Although the products of phase I reactions are more hydrophilic than the parent xenobiotics [12], the primary aim is to create reactive sites in the compound by addition or exposure of functional groups (hydroxyl or carboxyl) that will prepare the compound for phase II conjugation reactions. If the xenobiotic already contains a functional group for phase II metabolism, the detoxification will proceed without phase I metabolism.

- Phase II (conjugation): Phase II type of reactions accomplish the deactivation of xenobiotic or the phase I activated metabolite by conjugation (covalent linkage) to an endogenous hydrophilic molecule such as glucose, malonate or glutathione [13]. Halogen- and nitro-functional groups and the occurrence of conjugated double bonds trigger glutathione conjugation [14] resulting in a water-soluble conjugate compound. The increase in water solubility decreases the ability of the compound to partition in biological membranes, hence restricting its distribution within cells and tissues. Subsequently, water-soluble conjugates are exported to sub-cellular components by compartmentalization that prevents their interference with the activity of enzymes through product inhibition or their conversion to toxic metabolites by cytosolic enzymes [15, 16].
- Phase III (compartmentalization): Vacuoles and apoplasts are the sub-cellular compartments of the phase III processes [17]. The transport of the water-soluble conjugate from the cytosol to either the vacuole or the apoplast requires passage across the tonoplast or the plasma membrane. This is achieved by an ATP-dependent transporter which recognizes the glutathione conjugates as substrates [18].

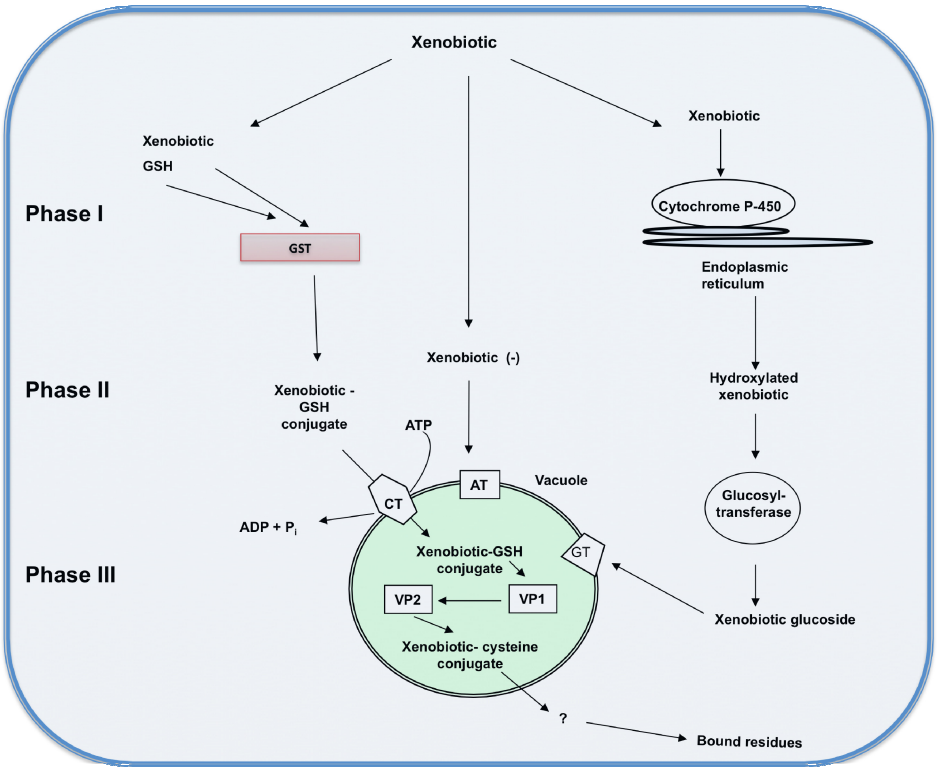

Figure 1. The enzyme-catalyzed reactions responsible for the detoxification of xenobiotics in plants. These reactions take place within several organelles and cellular compartments. Abbrevations: CT, glutathione-conjugate transporter; AT, ATP-dependent xenobiotic anion (taurocholate) transporter; GT, ATP-dependent glucose-conjugate transporter; VP, vacuolar peptidase. Adapted from [14].

1.1.2 GST-catalyzed conjugation of xenobiotics to GSH

GSTs are the principal phase II enzymes that catalyze the conjugation of activated electrophilic xenobiotics to the thiol of reduced glutathione, an endogenous water-soluble substrate [6]. The electrophilic sites necessary for GSH conjugation in xenobiotics are present in arene-oxides, aliphatic, aryl halides, α-β-unsaturated carbonyls, organonitro-esters and organic thiocyanates, while compounds such as haloalkanes, chlorobenzenes and thiocarbamates form the industrial substrates [4, 6]. The conjugation reaction proceeds with the displacement of a nucleophile (e.g. halogen or alkyl sulfoxide) (Fig. 2) [19]. The various reactions catalysed by GSTs include, for example, nucleophilic aromatic substitutions, Michael additions, epoxide ring-opening and isomerization reactions (Fig. 3) [20, 21].

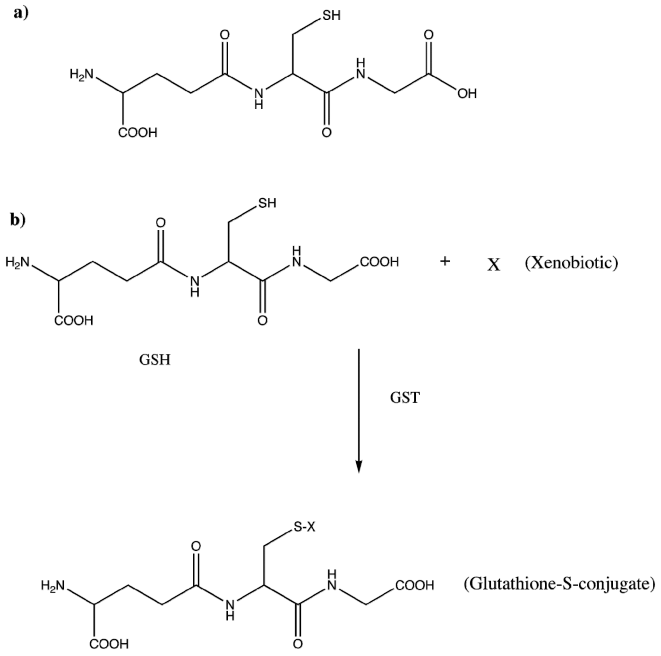

Figure 2. **(a)** Chemical formula of GSH (γ-Glu-Cys-Gly; γ-glutamylcysteinylglycine). **(b)** Glutathione conjugation to a generic xenobiotic (X) catalyzed by GST. The final product is a glutathione-S-conjugate.

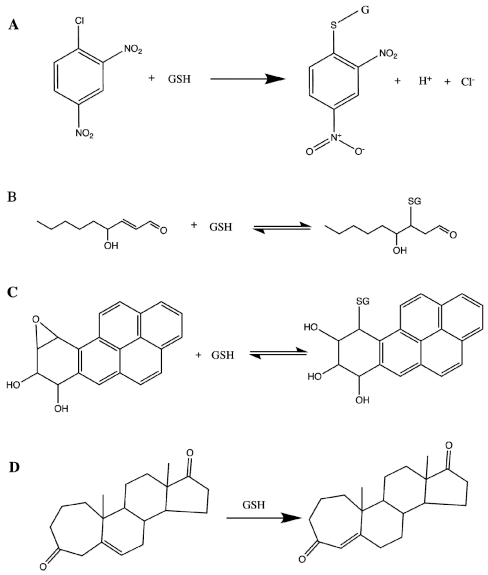

Figure 3. Typical GST-catalyzed reactions. **(a)** Nucleophilic aromatic substitution with 1-chloro-2, 4-dinitrobenzene, **(b)** Michael-type addition reaction, **(c**) epoxide-ring opening, **(d)** isomerization.

1.1.3 GST classification

Three GST subfamilies have been discovered so far: cytosolic, mitochondrial kappa, and microsomal. The subfamily of soluble cytosolic GSTs is the most abundant and omnipresent in all the aerobic organisms. There are 15-20 different GSTs occuring in mammals, including humans [22], 40-60 GSTs in plants [23], and more than 10 GSTs in insects [24]. The kappa GSTs are found in mitochondria and also in human peroxisomes [25]. The localization of the kappa GSTs in the organelles, which are known to be involved in lipid metabolism and the production of reactive oxygen species in large amounts, could suggest that the kappa GSTs are implicated in the role of detoxification of lipid peroxides in β-oxidation. Microsomal GSTs, now designated as membrane-associated proteins involved in eicosanoid and glutathione metabolism (MAPEG) exist in a wide spectrum of organisms, but are less numerous compared to cytosolic GSTs.

1.1.3.1 Cytosolic GSTs

Cytosolic GSTs (cGSTs) have been grouped into various classes (Table 1) based on several criteria, such as the amino acid and nucleotide sequence identity, physical structure of the genes (intron number and position), tertiary and quaternary structural properties, and immunoreactivity [4, 26]. Between members of the same class, the amino acid sequence identity is more than 40%, while between different classes it is less than 25% [27]. The mammalian-specific cGSTs that are recognized so far are Alpha, Mu, Pi, Sigma, Theta, Zeta, Omega, and Sigma. The six classes of plant-specific cGSTs are Lambda, Phi, Tau, Theta, Zeta, DHAR (dehyrdroascorbate reductases), and TCHQD (tetrachlorohydroquinone dehalogenase) [28]. The six insect specific classes are Delta, Epsilon, Sigma, Theta, Zeta, and Omega. The bacterial specific classes are Beta and Chi. Finally, the fungal GST classes are Alpha, Mu, and Gamma. Some of the monomer folds of the GST classes are shown in Fig. 4.

Table 1. Classes and biological functions of cytosolic GSTs [29].

Organism	Class	Function	Active site residues	Non-catalytic and/or specific functions
Mammalian	Alpha	Isomerase activities, drug metabolism, peroxidase activity, detoxification	Tyrosine	Signaling modulation
	Mu	Drug metabolism	Tyrosine	Signaling modulation
	Pi	Drug metabolism	Tyrosine	Signaling modulation
	Theta	Prevention of hepatocarcinogenesis, metabolism of industrial compounds	Serine	Prostaglandin synthesis
	Zeta	Catalysis of α-haloacids metabolism	Serine	Phe/Tyr catabolism; DCA dechlorination
	Omega	Oxidative stress	Cysteine	Ion-channels modulation
	Sigma	Prostaglandin synthesis	Tyrosine	Prostaglandin synthesis
Bacteria	Beta	Catabolism of organic compounds	Cysteine	
	Chi		Unknown	
Plants	Phi	Role in detoxification, oxidative stress protection, signalling, non-catalytic binding of flavonoids, participation in intermediary metabolism	Serine	Ligandin; signalling modulation
	Tau		Serine	Ligandin
	Theta		Serine	
	Zeta		Serine	
	Lambda		Cysteine	
	DHAR		Cysteine	
	TCHQD	Unknown	Possibly Serine	
Fungi	Alpha		Unknown	
	Mu		Unknown	
	Gamma		Unknown	
Insects	Delta	Possible detoxification of environmental xenobiotics	Serine	
	Epsilon	Detoxification of insecticides, peroxidase activity, oxidative stress	Serine	
	Theta	Unknown	Serine	
	Sigma	It probably acts against by-products of oxidative stress	Tyrosine	
	Zeta	Tyrosine degradation pathway	Serine	
	Omega	Unclear (probably act against oxidative stress)	Cysteine	

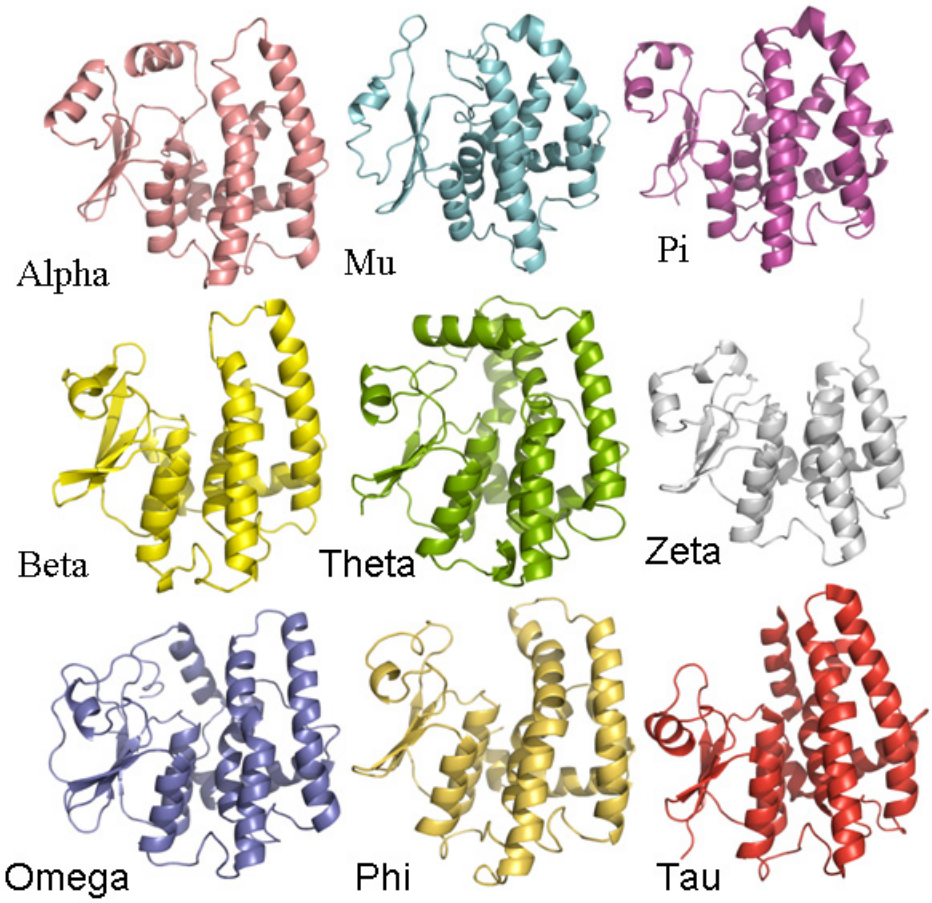

Figure 4. A comparison of the various monomer folds of the different classes of the GST superfamily. The structures from different classes were superimposed onto Tau class enzyme GSTU4-4 (PDB id: 1gwc [30]) using the program SSM [31] and displayed as differently colored individual ribbons for clarity. The structures superimposed are the mammalian Alpha, 1gse [32] (RMSD 3.2 Å for 187 residues); Mu, 4gst [33] (RMSD 2.6 Å for 179 residues); Pi, 1gss [34] (RMSD 2.5 Å for 181 residues); bacterial Beta, 1a0f [35] (RMSD 2.0 Å for 181 residues); plant Theta, 1ljr [36] (RMSD 2.5 Å for 196 residues); Zeta, 1e6b [37] (RMSD 1.9 Å for 171 residues); insect Omega, 1eem [38] (RMSD 2.1 Å for 198 residues) and Phi, 1gnw [39] (RMSD 2.1 Å for 187 residues).

1.1.3.2 Plant GSTs

The increasing interest in plant GSTs arises from herbicide selectivity and environmental safety. Plants are able to tolerate a wide spectrum of xenobiotics because of the broad-spectrum specificity of the GSTs. The different classes of herbicides metabolized by GSTs are triazines, thiocarbamates, chloroacetanilides, diphenylethers, and aryloxyphenoxypropionates. The primary basis of herbicide tolerance in plants is the differential ability of plant species to detoxify a herbicide (via GSH conjugation) in the resistant but not in the susceptible species. Plant GSTs also respond to plant hormones such as auxins and cytokines, to pathogenic infections,

oxidative stress and other conditions. They are capable of carrying out many more functions in addition to detoxification [40] such as homeostasis of hormones and catalysis of alternative GSH-dependent biotransformation reactions.

Plant GSTs are both cytosolic (soluble) and microsomal forming a complex superfamily of eight distinct classes, seven of which are soluble and one microsomal [28]. The microsomal GSTs are membrane-bound members of the MAPEG superfamily that catalyze GSH-dependent reactions [41]. The overall structure of the plant GSTs shows a high level of structural homology to those of animal origin.

1.1.3.3 Phi and Tau GSTs

The plant-specific Phi and Tau GSTs are primarily responsible for herbicide detoxification, displaying class specificity in substrate preference [42]. Phi class GSTs are highly active towards chloroacetanilides and thiocarbamate herbicides, whereas the Tau enzymes are efficient in detoxifying diphenylethers and aryloxyphenoxypropionates [43]. Phi and Tau classes of GSTs are dimeric and most abundant. They share functional similarity with the drug-metabolizing GSTs found in animals [28]. The Phi class of GSTs are the first class of enzymes of plant origin to be identified for their herbicide detoxification. Tau class GSTs were initially found to be induced by auxins. Later studies revealed their response to endogenous and exogenous stresses including pathogen attack, wounding, heavy metal toxicity, oxidative and temperature stresses [44]. The ability to bind hydrophobic substrates is much wider in plants than in mammalian enzymes [39, 45]. Apart from their primary role as detoxifying agents, these classes of GSTs also participate in endogenous cellular metabolism [39] by functioning as glutathione peroxidases that neutralize oxidative stress, as flavonoid-binding proteins [40], as stress-signalling proteins [46], and as apoptosis regulators [47].

1.1.4 3D structure

GSTs are composed of 200-250 amino acids with a molecular mass ranging from 20–28 kDa [4, 48-50]. Structural studies of the various cGSTs of plant, animal and bacterial origin have shown a striking level of structural conservation in fold and dimeric organization. Therefore, all the GSTs are characterized by a two-fold axis and pose an independent binding site in each subunit (Fig. 5a). The basic GST fold of each subunit contains two domains: an N-terminal domain and a C-terminal domain. The N-terminal domain consists of α helices and β strands and adopts a thioredoxin-like (TRX) fold (βαβαββα) [51], which is also shared by glutaredoxin and glutathione peroxidase [52]. The two structural motifs of the N-terminal domain are made up of the N-terminal β1α1β2 and the C-terminal β3β4α3, which are linked together by a long loop that hosts the α-helix α2. Thus, three parallel β-strands β1β2β4 and the single antiparallel β3 form a β-sheet sandwiched between the α-helix α2 on one side and α-helices α1and α3 on the other side (Fig. 5b). The presence of a *cis*-Pro loop connecting the α-helix α2 and the β3-strand is observed in all the GSTs [53]. The conserved *cis*-Pro loop is probably important for the recognition of and subsequent binding to GSH [54].

The C-terminal domain is all α-helical and is connected to the N-terminal domain by a short linker sequence of ~ 10 residues. Unlike the N-terminal domain, the C-terminal domain is quite variable with respect to sequence and topology thus leading to distinct hydrophobic substrate specificities. Moreover, plant GSTs possess a larger cleft for co-substrate binding compared with mammalian GSTs and hence have the ability to accept a larger and much more diverse variety of substrates. The type of interactions between the two subunits involved in the assembling and maintenance of the quaternary structure varies amongst different classes of GSTs. The interactions are hydrophobic in Theta, Sigma, Beta, and Tau classes and hydrophilic in Alpha, Mu, Pi, Phi, and Omega classes.

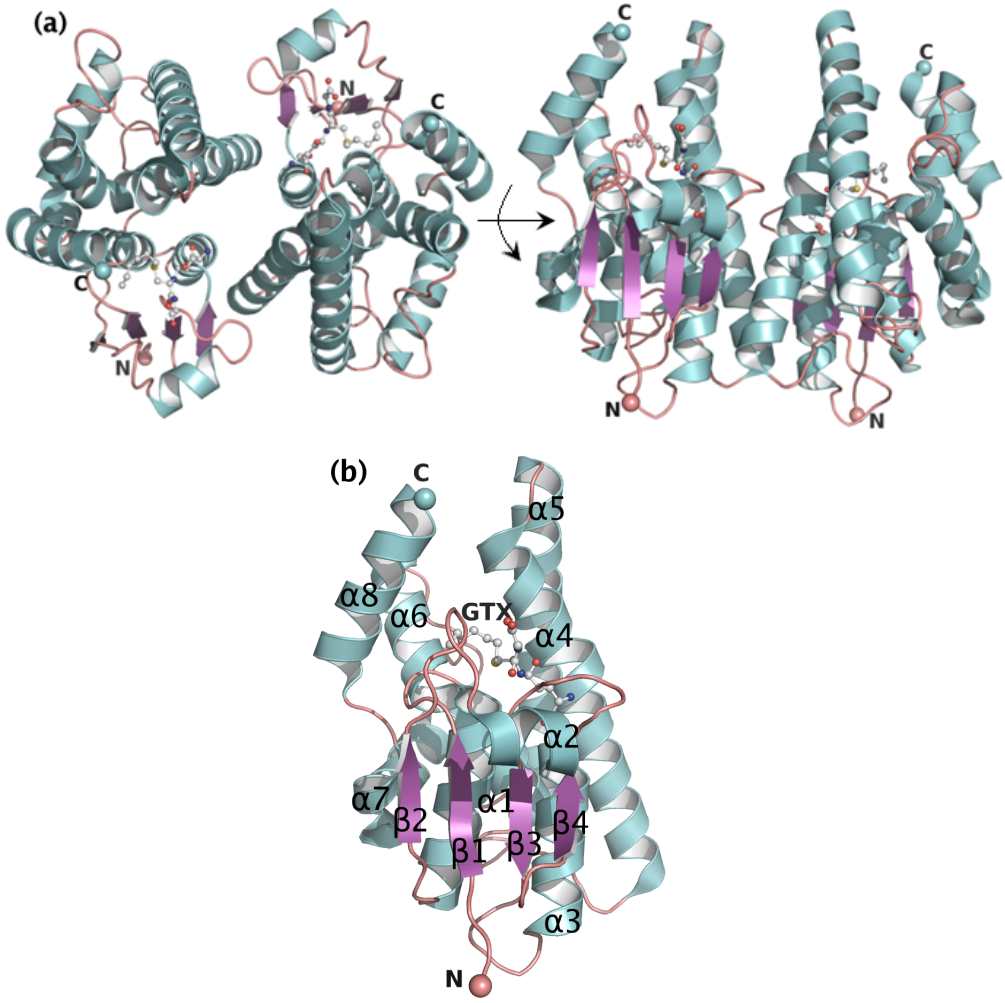

Figure 5. **(a-left**) Cartoon diagram of dimeric Tau GST (PDB id: 1gwc [30]). **(a-right)** The dimer after 90° rotation. **(b)** Cartoon representation of Tau class monomer. The colouring scheme is according to secondary structural elements. The active site is occupied by S-hexylglutathione (GTX), which is shown as ball-and-stick representation and coloured according to atom type. The Figure was created by PyMol (http://www.pymol.org).

1.1.4.1 Active site

The active site is formed by residues from the N- and C-terminal domains. It comprises two sub-sites: a glutathione-specific site (G-site) constructed from residues of the N-terminal domain, and a hydrophobic substrate binding site (H-site) formed by non-polar side-chains of the C-terminal domain. A conserved Tyr residue in the active site of mammalian Alpha Mu and Pi classes and a conserved Ser in Theta, Zeta, Phi, Tau and Delta classes (Fig. 6) are involved in the catalytic activation of GSH by acting as hydrogen bond donors to the thiol group of the GSH. This leads to the formation and stabilization of the highly reactive thiolate anion which is susceptible to a nucleophilic attack by an electrophilic substrate [5, 55, 56]. The amino acid sequence alignment between the Phi and Tau GST classes has revealed a highly conserved nature of the N-terminal G-site for GSH binding and of the C-terminal for co-substrate binding. A ligand binding L-site is observed in a hydrophobic surface pocket in some classes of GSTs. For example, the human P1-1 enzyme binds part of the compound sulfasalazine in the L-site [57].

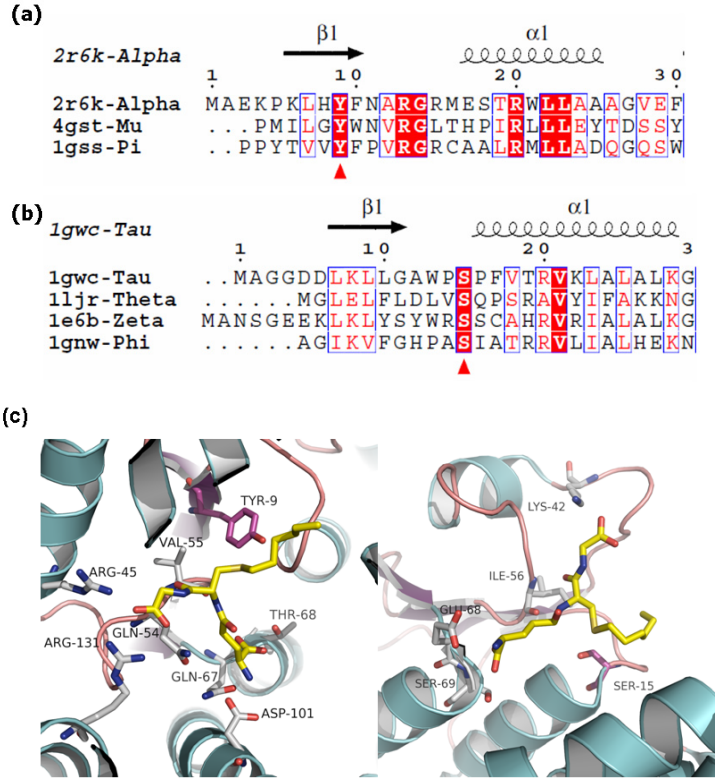

Figure 6. **(a)** Multiple sequence alignment of Alpha (2r6k [58]; NCBI code: AAA70226), Mu (4gst [33]; AAA41293) and Pi (1gss [34]; CAA29794) classes showing the conserved 2r6k-Tyr9 that is marked. **(b)** Multiple sequence alignment of Tau (1gwc [30]; AAM89393), Theta (1ljr [36]; AAB63956), Zeta (1e6b [37]; AAG30131) and Phi (1gnw [39]; AAA32800) classes. The conserved Ser15 is marked. **(c)** Close-up view of the active sites of (left) Alpha (2r6k) and (right) Tau (1gwc) classes. The active site residues and GTX in both the structures are shown in stick representation and coloured according to atom types. The active site Tyr9 and Ser15 are shown in different colours.

1.1.5 Biotechnological applications

The development of inventive remediation technologies is of paramount importance since these technologies help combat the environmental pollution created by organic xenobiotics such as pesticides, pharmaceuticals and petroleum products [59]. The use of plants to clean up polluted soils and water (phytoremediation) has been recognized as a cost-effective method of decontaminating soil and water resources [60]. The fact that plants exhibit a variety of pollution attenuation mechanisms renders them more feasible than physical or chemical remediation means [61, 62].

Although plants possess the inherent capability to detoxify xenobiotics, they are deficient in the catabolic pathways to degrade these compounds completely compared to the microorganisms. On the other hand, microorganisms are not preferred for the remediation of xenobiotics as they require both inoculation and nutrient application for efficient functioning. Besides, microbes that exhibit considerable biodegradation efficiency in the laboratories, fail to exhibit the same at actual contaminated sites. A greater concern with respect to plants is also the introduction of contaminants in the food chain. Therefore, a direct method for enhancing the efficacy of phytoremediation is via transgenesis by overexpressing in plants the genes involved in metabolism, uptake, or transport of specific pollutants [63]. The insertion of multiple genes for phase I metabolism (cytochrome P-450s) and phase II metabolism (GST, GT etc) for complete degradation of the xenobiotics within the plant system is one of the most promising methods of transgenic technology.

1.1.5.1 Transgenic plants

Transgenic organisms assist in understanding the gene functions *in vivo*, in setting up "cell factories" for the production of compounds of medical and technological applications, and in engineering organisms with new desirable characteristics. Furthermore, creating bacterial strains for the degradation of toxic/carcinogenic compounds is another active area of research [49].

GST from maize was the first of its kind to be exploited owing to its participation in herbicide (atrazine) metabolism [64]. Since then, several successful approaches have been reported for the generation of transgenic plants overexpressing GST isoenzymes. Some examples are given below:

- The bacterial gene encoding γ-glutamyl-cysteine-synthetase (γ-ECS), a rate-limiting regulatory enzyme in the biosynthesis of GSH, was overexpressed in poplar plants (*Populus balsamifera*) [65]. Enhanced levels of GSH and its precursor γ-EC were observed in the transformed plants. The increased levels of GSH eventually led to the protection of plant cells from oxidative stress due to environmental factors. Enhanced tolerance to atrazine, CDNB, metachlor and phenantrene were also observed in γ-ECS- and GST-overexpressing *Brassica juncea* [66].
- Transgenic tobacco (*Nicotiana tobaccum*) plants expressing the *gst1* gene from maize were developed. The transgenic plants exhibited higher tolerance to

alachlor in terms of root, leaves and vigorous development compared to non-transgenic plants [67].

- Cytochrome P4502E1 gene from human involved in the phase-I of the organic pollutant degradation and GST gene from fungus *Trichoderma virens* involved in phase-II detoxification were inserted into *Nicotiana tobaccum [68]*. The transgenic plants exhibited enhanced degradation of anthracene and chloropyriphos.

1.1.5.2 Biosensors

The principal role of GSTs in xenobiotic-GSH conjugation has formed the basis for the development of novel biosensors. Herbicide determination via biosensors is considered environmentally safe and requires minimum sample preparation without compromising the accuracy [69]. Two examples are given below:

- Acrylamide detection in starchy foods. The *gst-4* gene from *Caenorhabditis elegans* was selected to construct a *gst-gfp* fusion gene that was used to transform *C. elegans* into a biosensor [70]. The GFP signal is not emitted in the absence of acrylamide while a very strong signal is emitted from the whole body of *C. elegans* in the presence of acrylamide.
- Captan detection. Captan, a non-systemic fungicide, is a powerful carcinogen and harmful chemical to the water ecosystem [71-73]. An optical biosensor consisting of GST-immobilized gel film was constructed for quick, simple, and sensitive detection (up to 2 ppm) of captan in water supplies [69].

1.1.6 Biomedical applications

GSTs are of immense interest in the fields of pharmacology and toxicology because they metabolize diverse chemicals such as cancer chemotherapeutic agents, carcinogens, and insecticides and, therefore, provide targets for asthma and antitumor drug therapies. Importantly, overexpression of GSTs in mammalian tumour cells that exhibit resistance to various anti-cancer agents has been observed [22].

1.1.6.1 Diagnostics

Soluble cGSTs can be used in diagnostics and in monitoring the clinical course of cancer. The increase in expression of GSTs as the tumour progresses could be exploited as a useful immunological marker for many cancers. Some examples of the applications of GSTs in diagnostics include:

- An increase in the levels of GSTP1-1 was observed in patients with gastric cancer and gliomas as the tumour progresses. Hence, GSTP1-1 could be used as a marker for gastric cancer progression [74].
- Epidemiological studies have implicated polymorphisms of human GST genes as a response to cancer therapy [75]. Accordingly, the subtypes and the variants of GSTs could become potential drug targets in cancer therapy [76, 77].

- The diagnostic applications of GSTs extend to avenues other than cancer, as well. Elevated levels of plasma Pi GST were found in chronic hepatitis, chronic cholestatic diseases, primary biliary cirrhosis and transplant rejection. Hence, GST measurements in plasma might be useful in assessing the hepatic status [78].
- The Omega class of GSTs (GSTO) hosts a special range of enzymatic activities compared to other GSTs. The isoenzyme GSTO1-1 exhibits dehydroascorbate reductase and thioltransferase activities while catalysing the reduction of monomethylarsonate, an intermediate in the arsenic biotransformation pathway [38]. The human GSTO1-1 is involved in the modulation of ryanodine receptors and interacts with cytokine release inhibitory drugs. In addition, GSTO1 is also linked to both Alzheimer's and Parkinson's diseases [79].

1.1.6.2 Drug design

GSTs are involved in the efficient detoxification of several chemotherapeutics and are therefore, considered as crucial factors in regulating the susceptibility to cancer [80]. An elevated level of GSTs was observed in cancer cell lines compared with the parental cells lines and the normal tissues [81, 82].

The overexpression of GSTs, particularly the GSTP1-1 isoform, observed in neoplastic cells in cancers resistant to drugs can be used as a platform for pro-drug development. An interesting example of a pro-drug is TLK286, which is activated by GSTP1-1 [83]. The drug binds at the active site of human GSTP1-1 and is activated by Tyr7 through a β-elimination reaction.

GSTs can also be used as potential drug targets in diseases other than cancer. The present therapy for schistozomiasis occurs via a drug (oltipraz) that binds directly to the GST of the integument of the nematode [84]. The low homology between the human and parasitic GSTs (<30 %) is the key factor for drug design. Differences in their respective hydrophobic clefts have been observed with a more open cleft in the former [85].

1.2 L-Asparaginases

The L-asparaginase activity in the blood of guinea pig serum was first discovered by Clementi in 1922 [86] and after 40 years [87] it was found responsible for the antitumour properties of the guinea pig serum [88]. Subsequently, potent antileukemic L-asparaginases were found in bacteria and introduced into clinical practice especially for the treatment of acute lymphoblastic leukaemia (ALL) [89-91]. The role of L-asparaginase (EC 3.5.1.1) in the treatment of ALL is accredited to the fact that the tumour cells have a compromised ability to generate L-asparagine necessary for cellular functions to keep up with their malignant growth [92]. This could be either due to low expression levels of asparagine synthetase [93], or to insufficient supply of its substrates, aspartate or glutamine [94]. The cancerous cells thus depend on extracellular supply of L-asparagine for protein, DNA and RNA synthesis and G1 phase of cell division. The enzyme, however, selectively starves cancerous cells

leaving out the normal cells, which are capable of synthesizing the necessary amount of the amino acid for growth with the help of asparagine synthetase [92].

1.2.1 General reaction mechanism catalyzed by L-asparaginase

The reaction catalyzed by L-asparaginase is a simple hydrolysis of the side-chain amide bond of L-asparagine. The reaction can be assayed by measuring the release of ammonia in a simple Nessler test [95]. The reaction mechanism is similar to the two-step mechanism of serine proteases that involves three residues forming a catalytic triad : a nucleophile, a general base and an additional acidic residue [96]. In serine proteases, the catalytic triad is typically Ser-His-Asp. In L-asparaginases the reaction proceeds as follows [97] (Fig. 7):

- Step 1: In the beginning, the nucleophile is activated via a OH…B hydrogen bond to the adjacent basic residue. The C atom of the amide substrate is then attacked leading to the formation of an acyl-enzyme intermediate through a tetrahedral transition state. Stabilization of the negative charge that develops on the O atom of the amide group during the transition state is achieved by an 'oxanion hole' resulting from the interaction with adjacent hydrogen bond donors (main-chain N-H groups).
- Step 2: The second step proceeds in a similar way to the first except that the initiation of the attack on the ester C atom (Asp) is now carried out by an activated water nucleophile.

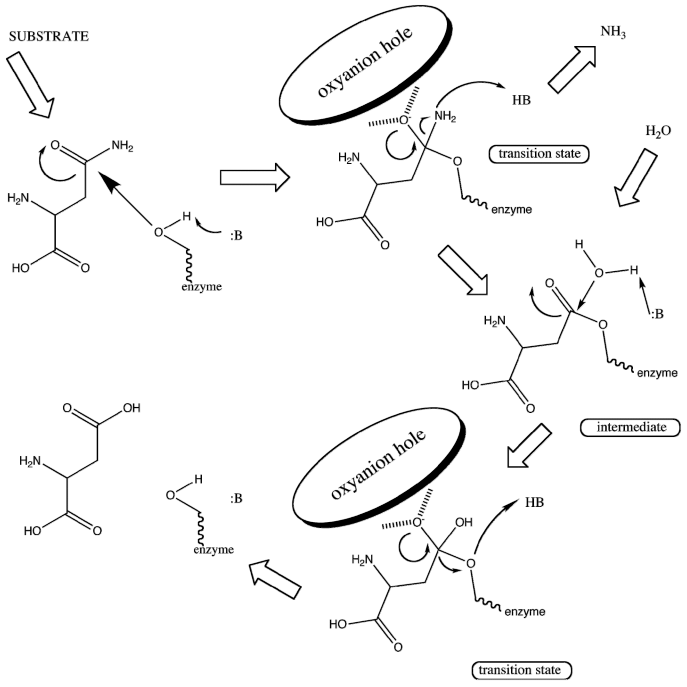

Figure 7. Proposed general mechanism of L-asparaginase catalytic reaction (adapted from [97]).

1.2.2 Sources of L-asparaginases

The demand for large amounts of the enzyme for clinical studies has promoted the search for new L-asparaginases. L-asparaginases from various organisms such as microorganisms, mycobacteria, yeast molds, plants and plasma of some vertebrates have been isolated and characterized [98-100]. The native forms of L-asparaginase have been isolated from a number of bacteria. Among them, L-asparaginase from *Escherichia coli* (EcAII) and *Erwinia chrysanthemi* (ErA) were found to be useful from a clinical point of view [101]. Subsequently, two isoenzymes produced in *E. coli* were discovered and designated as type-I and type-II L-asparaginase [102]. Structural aspects of *E. coli* type-II and -I L-asparaginases are discussed under sections 1.2.4.1 and 1.2.4.2, respectively.

1.2.3 Treatment and side-effects

Natural enzymes used as therapeutic drugs have to be purified extensively to eliminate toxic reactions and increase their persistence in the circulation for prolonged period of time. Two bacterial L-asparaginases, EcAII and ErA, have successfully overcome the above mentioned challenges and have major applications in the treatment of ALL [103]. Randomized clinical trials have suggested that the clinical efficacy of EcAII is superior to that of ErA. Despite the achieved success rate in the treatment of childhood ALL, EcAII and ErA exhibit a unique toxicity profile with EcAII characterized by greater toxicity due to induction of increased coagulation abnormalities. Vomiting and allergic reactions are the mild side-effects, while the life-threatening adversities such as hypersensitivity, pancreatitis, clotting of large veins, liver toxicity, hyperglycemia, neuropathy, and reduced clotting factors with bleeding are more severe side-effects [104]. Some adversities arise mainly due to the intrinsic glutaminase activity (the glutaminase activity for EcAII and ErA amounts to 2 % and 10 % of their asparaginase activity, respectively) [105]. The low half-life of EcAII (Table 2) further decreases its potential as a chemotherapeutic agent. In order to overcome the above limitations, EcAII has been pegylated.

Covalent linkage to polyethylene glycol (PEG) generally prolongs the plasma retention time of the enzyme and also decreases the loss of the enzyme due to proteolysis and renal excretion [106]. Pegylated L-asparaginase (PEG-ASP) has a prolonged half-life (5.5 days), and is associated with decreased immunogenicity compared with that of EcAII [107, 108]. The efficacy, safety and tolerability of PEG-ASP have been demonstrated by clinical trials [109].

PEG-ASP shares similar chemical properties with EcAII, with optimal conditions for activity at pH 7.0, isoelectric point at pH 5.0 and reaction temperature of 50 °C [110]. PEG-ASP can be given to children with a history of allergic reactions to previous administration of EcAII and is prescribed to patients who require L-asparaginase but have developed resistance to the native form [111]. The major side-effects due to the administration of PEG-ASP are similar to those of native enzyme and are related to the inhibition of normal protein synthesis (including the production of

fibrinogen, antithrombin III, protein C and S, along with other clotting factors), and the development of anti-asparaginase antibodies [110]. Therefore, an L-asparaginase that can overcome all the above-mentioned limitations is desirable for the treatment of childhood ALL.

1.2.4 *E. coli* L-asparaginases

The two isoenzymes of L-asparaginase that are expressed in *E. coli* are known as type-I and type-II. The percentage sequence identity between them is 24% (Fig. 8). The type-I L-asparaginase (EcAI) is expressed constitutively whereas the type-II L-asparaginase (EcAII) which has a tumour-inhibiting effect is expressed under anaerobic conditions [112]. EcAI displays lower affinity for the substrate (K_m = 5 mM) [113] compared to its type-II counterpart (K_m = 11.5 μM) [114].

Table 2. Preparations of L-asparaginases [115]

Form of L-asparaginase	Properties	Half-life (days)[#]
E. coli	Native form; it can induce hypersensitivity reactions	1.28 ± 0.35
E. chrysanthemi	Minimal cross-reactivity with *E.coli* preparation; shortest half-life	0.65 ± 0.13
PEG-ASP	Decreased immunogenicity; longer half-life	5.73 ± 3.24

[#]Intramuscular administration.

Although these two enzymes catalyze an identical reaction, they can be distinguished by their solubilities in ammonium sulphate solution and by their sensitivity to thermal activation [102].

Structural details of only a few type-I L-asparaginases are available because of their lack of therapeutic applications. Although the short half-life of the enzyme (15 min) may explain its inactivity in animal models, the inactivity in cell culture still remains a mystery. The biochemical properties that are mostly responsible for the above include high K_m value for L-asparagine, the substrate specificity or potential allosteric kinetics. The type-II L-asparaginases, on the other hand, are more extensively studied at both structural and mechanistic levels.

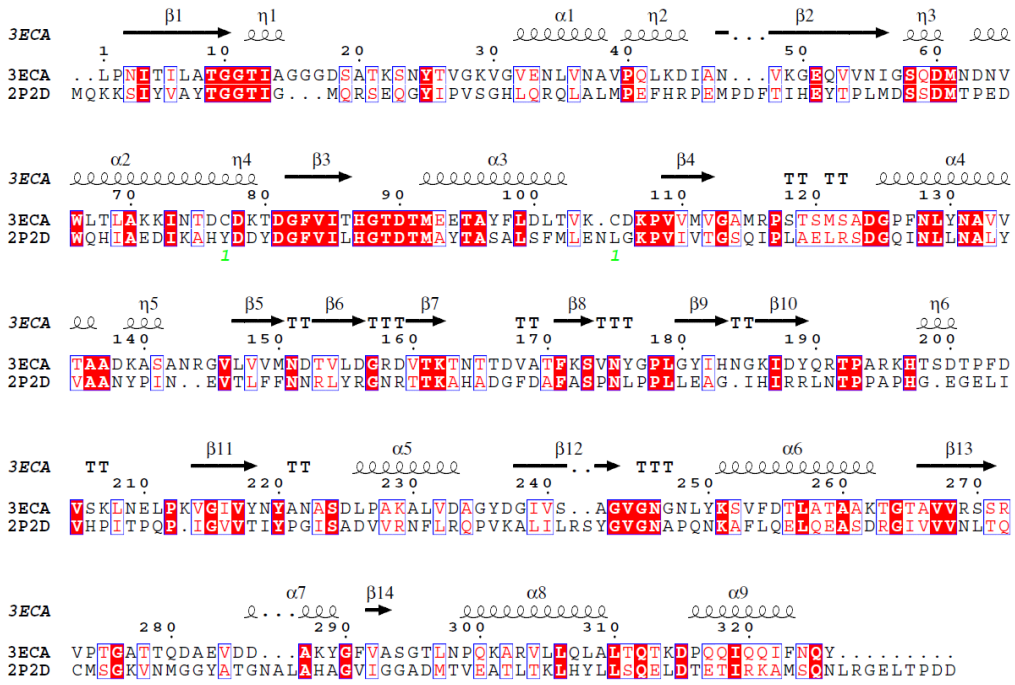

Figure 8. Sequence alignment between the EcAII (PDB id 3eca [116]; AAA23445.1) and EcAI (PDB id: 2p2d [117]; ACX39533) L-asparaginases. The position of the disulphide bridges is depicted in green.

1.2.4.1 Structural details of type-II L-asparaginases

Structural studies of type-II L-asparaginases have been conducted on a number of bacterial species including *E. coli* [116], *Erwinia chrysanthemi* [101, 118, 119], *Acinitobacter glutamininasificans* [120], *Pseudomonas 7A* [120], *Erwinia carotovora* [121, 122], and *Wolinella succinogenes* [123]. Thirty-nine refined crystal structures till date are available in the Protein Data Bank for substrate-free forms, various mutants, complexes and reaction intermediates of L-asparaginases. The structural studies have revealed that the bacterial type-II L-asparaginases are active as tetramers of identical subunits that obey the 222 symmetry (Fig. 9a). Each subunit consists of ~ 330 amino acids with a molecular weight of approximately 35 kDa. Crystal structures of EcAII [116] and EcAII T89V variant together with kinetic data [124, 125] that facilitated the identification of the residues involved in substrate binding and catalysis.

The active site is located between the N-terminal domain of one subunit and the C-terminal domain of another (Fig. 9b). A pair of Thr residues (EcAII Thr12 and Thr89) is located on either side of the scissile bond of the substrates. The formation of a Thr12-acyl complex has led to the suggestion that Thr12 and not Thr89 is the primary nucleophile in the L-asparaginase reaction. Thr12 along with Tyr25 are part of the flexible loop that attains stability upon substrate binding [126]. The other part of the active site is rigid and comprises Thr89, Asp90 and Lys162. Glu283 from the adjacent subunit plays a crucial role by assisting in substrate binding.

A left-handed crossover connecting the β4 and β5 strands in the N-terminal domain is observed in all the L-asparaginases. Such crossovers are rarely observed and are considered to be important for the enzymatic catalysis. The residues involved in the crossover form a part of the active site. Furthermore, the amino acid residues that comprise the crossover are evolutionarily conserved because they provide a substantial part of the interface between the pairs of dimers in the tetramer [119]. The formation of a hydrogen bond between the carbonyl O atom of EcAII Ala20 from the active-site flexible loop and the main-chain N atom of Leu127 from the crossover is characteristic of all L-asparaginases.

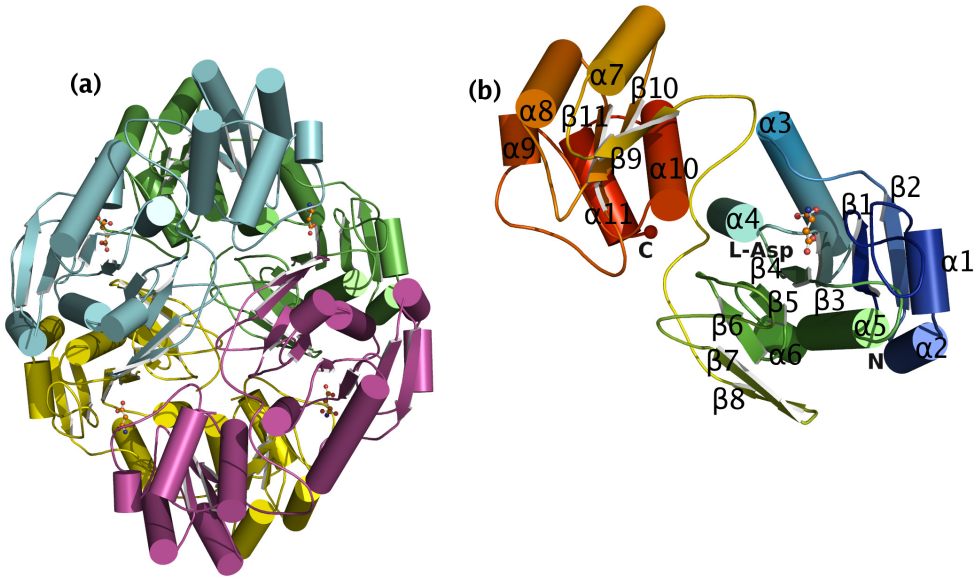

Figure 9. **(a)** The tetramer of EcAII (PDB id: 3eca) where the helices are shown as cylinders and the A, B, C and D subunits are coloured green, turquoise, magenta and yellow, respectively. L-asparate is shown in ball-and-stick representation and coloured according to atom types. **(b)** Monomer of EcAII where the secondary structure elements are labelled. The colouring scheme is from blue (N-terminus) to red (C-terminus). The active site is occupied by L-aspartate, which is represented as ball-and-stick and coloured according to atom types.

1.2.4.2 Structural details of type-I L-asparaginase

The crystal structure of type-I EcAI in the presence of L-Asn has been determined at 1.9 Å [117]. The structural analysis revealed a tetramer in the asymmetric unit. The overall structure of EcAI is very similar to the related L-asparaginases (Fig. 10a) and also includes the left-handed crossover structural motif. The α/β domains of the molecule are connected by an extended but structured linker region from residue 191 to 210. The unexpected feature of the complex is the location of four tightly bound asparagine molecules at equivalent locations within the tetramer, far from the active site (Fig. 10b). The distance between the Cα-atoms of the bound asparagine residues within the dimer is less than 7 Å. It was suggested that asparagine might have a dual

role as a substrate and as an allosteric effector molecule. The putative allosteric site is located at the N-terminus of α-helix α8 and close to the dimer interface. Kinetic, mutagenic and hydrodynamic experiments supported further the notion of an allosteric switch in EcAI [117].

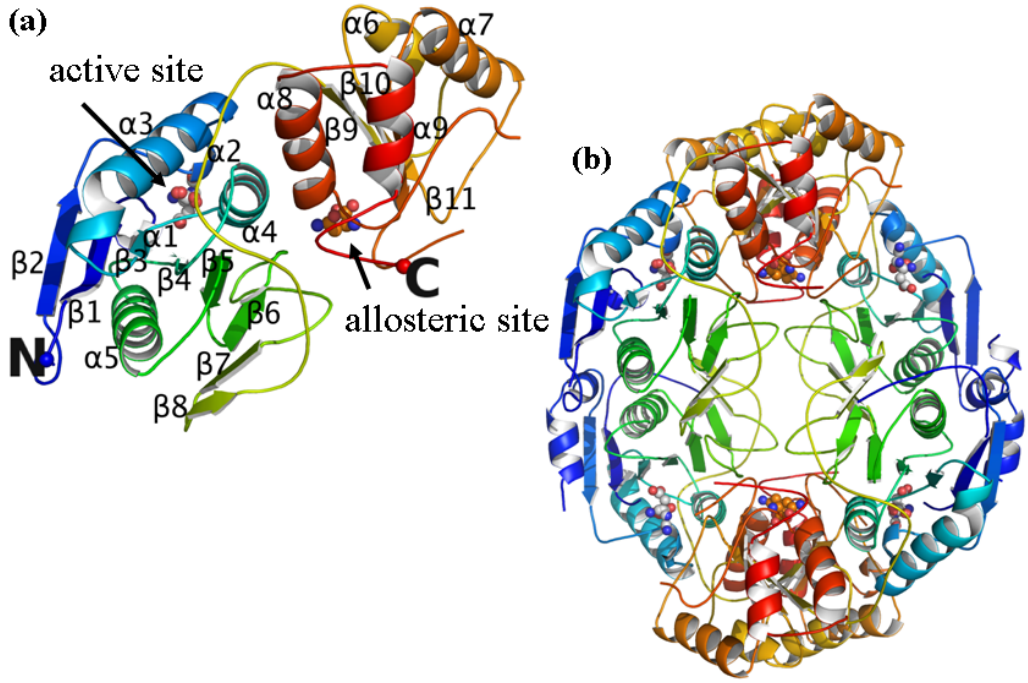

Figure 10. **(a)** Cartoon representation of the monomer of EcAI (PDB id: 2p2n [117]) depicting the secondary structure elements. The colouring scheme is from blue (N-terminus) to red (C-terminus). The active site (light colour) and allosteric site (dark colour) are occupied by L-aspartate, represented by space-filling models and labelled. **(b)** Similar representation of EcAI tetramer.

1.2.5 *Helicobacter pylori* L-asparaginase

Currently, two L-asparaginases (91% sequence identity) from different strains of the pathogenic bacterium *Helicobacter pylori* have been studied in detail. Strain J99 L-asparaginase (HpA) is the subject of the structural studies in this thesis. A functional study of the second L-asparaginase (*Helicobacter pylori* CCUG 17874 strain) has been carried out independently to gain insights into the pathological and therapeutic properties of the enzyme [127]. An important feature of these two L-asparaginases is their negligible (0.01%) L-glutaminase:L-asparaginase activity compared to the other type-II enzymes. Moreover, the enzyme was found to exhibit the following important properties that could make it a chemotherapeutic candidate:

- Positive homotropic cooperativity towards L-glutamine that can account for its lower affinity for L-glutamine compared to other type-II L-asparaginases.

- High thermal stability showing a T_{50} of 53 °C strengthening its suitability to chemotherapeutic usage.
- A sigmoidal pH rate profile against L-asparagine with a broad optimum in the pH range of 7.0-10.0 in contrast to the bell-shaped pH rate profile for L-glutamine with the maximum activity at pH 7.5.
- High cytotoxic activity towards several humoral cell lines (HL60, MOLT-4, HDF, AGS, MKN28, MKN74, and MKN7).

2 AIMS OF THE PRESENT STUDY

The aim of this thesis was to characterize a fluorodifen-inducible GST from *Glycine max* complexed with glutathione and S-(p-nitrobenzyl)-glutathione and to obtain structural and functional information of L-asparaginase from *Helicobacter pylori* strain J99. The specific goals were:

I GST
- To produce crystals of complexes of GmGSTU4-4 with glutathione and S-(p-nitrobenzyl)-glutathione.
- To determine the crystal structures of the two complexes.
- To compare the structures and study molecular recognition, binding, and catalytic aspects.

II L-asparaginase
- To crystallize HpA.
- To determine the three-dimensional X-ray crystal structure.
- To explore the active site of the enzyme and understand the behaviour of the flexible loops near the active site.
- To compare the structure with the other type-II L-asparaginases to better understand the catalytic mechanism and specificity of the enzyme.

3 SUMMARY OF MATERIALS AND METHODS

3.1 Crystallization

Prior to crystallization screening, the purified proteins supplied by our collaborators were concentrated by ultrafiltration using Amicon YM-10 filters in an appropriate exchange buffer and the concentrated protein was then stored in the same buffer. The concentration of the protein was measured by the Bradford method using bovine serum albumin as a standard [128]. Screening of the crystallization conditions was done by PACT (Qiagen) and INDEX (Hampton Research) screens on 96-well Corning plates by the sitting-drop vapour-diffusion method at +16 °C. Typically, a 1.0 µl of the protein was mixed with an equal amount of the crystallization solution in the respective well and incubated at +16 °C. Optimization of the crystallization condition that produced crystals was carried out by the hanging-drop vapour-diffusion method by equilibrating 2 µl of the protein mixed with an equal amount of the precipitant solution taken from a reservoir of 800 µl (Fig. 11).

3.1.1 GST-GSH complex

Purified *Gm*GSTU4-4 was concentrated to 12.5 mg/ml in 10 mM HEPES-NaoH at pH 7.0 and 10 mM GSH was added to the concentrated protein. Condition No. 20 (tri-sodium citrate 1.4 M, 0.1 M HEPES-NaOH, pH 7.5) of the INDEX screen yielded the first crystals and the condition was further optimized by the hanging-drop vapour-diffusion method. The optimal condition (tri-sodium citrate 1.2–1.3 M in 0.1 M HEPES-NaOH, pH 7.4 at 16 °C) produced crystals within 1 day. The crystals attained a maximum size of 0.5×0.15×0.15 mm^3 within 3 days.

3.1.2 GST-Nb-GSH complex

Previously purified and concentrated GmGSTU4-4 was mixed with a stock solution of S-(p-nitrobenzyl)-glutathione (100 mM in 0.1 M Na/K phosphate buffer, pH 7.0) to a final concentration of 10 mM. Condition No. 70 (0.2 M NaCl, 0.1 M Bis-Tris, pH 5.5, 25% (w/v) PEG 3350) of the INDEX screen resulted in the appearance of crystals. X-ray diffraction quality crystals were grown within four to five days under the same conditions without further optimization.

3.1.3 HpA

The protein was concentrated to 3.7 mg/ml as measured by the Bradford method and stored in the presence of 10 mM HEPES-NaOH, pH 7.0. Crystals appeared after 2 days under condition No. 92 of the INDEX screen that consisted of 15% (w/v) PEG 4000 and 0.1 M magnesium formate. Optimization of condition 92 resulted in good quality crystals that appeared within 4 days under the following conditions: 17.5% (w/v) PEG 4000, 0.1 M Mg formate, 0.1 M HEPES-NaOH, pH 7.0.

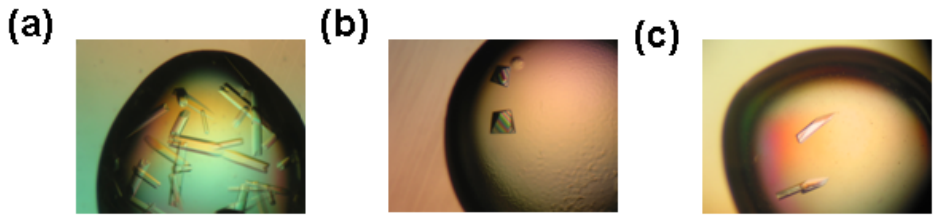

Figure 11. Typical crystals of **(a)** GmGSTU4-4-GSH, **(b)** GmGSTU4-4-Nb-GSH, and **(c)** HpA.

3.2 Data collection and processing

3.2.1 GST-GSH complex

Cryogenic data to 2.7 Å resolution were collected from a single crystal on station X13 in EMBL-Hamburg, c/o DESY by using 20% (v/v) glycerol as a cryoprotectant and subsequent flash-cooling in a gaseous nitrogen stream at 100 K. Despite their relatively big size, the crystals diffracted weakly owing to their high solvent content (74%) as deduced by the Matthews coefficient (V_m = 4.86 $Å^3$ Da^{-1}). A 2-min exposure time was used in order to record weak high-resolution reflections. Data processing was carried out using the HKL suite [129].

3.2.2 GST-Nb-GSH complex

Data under cryogenic conditions were collected up to 1.75 Å from a single crystal on station X11 in EMBL-Hamburg. Mother liquor solution containing 20% (v/v) glycerol was used as a cryoprotectant where the crystal was briefly soaked prior to data collection. The raw diffraction data were indexed, integrated, scaled and merged using the HKL suite.

3.2.3 HpA

An in-house data set to 2.6 Å resolution was initially collected from a single crystal soaked for a few seconds in a mother liquor solution containing 25% (v/v) glycerol as a cryoprotectant. The crystal was subsequently flash-cooled at 100 K in a gaseous nitrogen stream. Higher resolution cryogenic data (1.4 Å) were collected on station X13 (λ=0.8081 Å) at EMBL-Hamburg. In addition, a room-temperature dataset to 1.8 Å resolution was collected on X13 from a single crystal mounted on a quartz capillary. All data were indexed, processed and scaled using the HKL package. Data collection and refinement statistics are shown in Table 3.

3.3 Structure determination and refinement

All the structures in the present study were determined by molecular replacement using PHASER [130] in the CCP4 programme suite [131]. Inspection of the 2|Fo|-|Fc| and

|Fo|-|Fc| maps and manual model building was performed by COOT [132]. A randomly selected subset (5%) of the total number of reflections was set aside for cross-validation analysis to monitor the progress of refinement using the R_{free} factor. The co-ordinates were submitted to Translation/Libration/Screw Motion Determination TLSMD server [133, 134] for protein partitioning to perform TLS and restrained refinement in REFMAC [135]. Various aspects of manual modelling such as the side-chain flip in Asn and Gln residues, alternative conformations, and addition of solvent molecules were carried out. Waters with B-factor higher than 60 $Å^2$ were removed from the structures during the course of the refinement.

3.3.1 GmGSTU4-4-Nb-GSH complex

A poly-alanine model of the rice GST structure (PDB id: 1oyj, with 47% sequence identity) [136] was used as a search model for molecular replacement. The best solution was obtained in $P4_12_12$ spacegroup, thus resolving the ambiguity in the space group. The model was submitted to ARP/Warp for automatic building of the side-chains. Structural refinement was carried out by REFMAC in CCP4.

3.3.2 GmGSTU4-4-GSH complex

The poly-Ala model derived from the coordinates of GmGSTU4-4-Nb-GSH was used as a search model for molecular replacement to determine the GmGSTU4-4-GSH structure. The best solution with a Z-score of 61.4 was obtained in $P6_1$ space group and selected for refinement by REFMAC and subsequent rebuilding.

3.3.3 HpA

A poly-Ala model of the A subunit of *Wolinella succinogenes* L-asparaginase (PDB id: 1wsa; 55% sequence identity with HpA) [123] was used as a search molecule for molecular replacement. A Z-score of 22 was observed for the top solution employing the 2.6 Å resolution in-house data. REFMAC in CCP4 was initially used to carry out the refinement. The resolution was extended to 1.4 Å when the new data set became available. Anisotropic refinement was carried out by SHELXL-97 during the final stages of refinement [137]. Default values for the distances, planarity, chiral and anti-bumping restraints by SHELX-97 were used for the protein molecules. Geometric restraints for the ligand were generated by the PRODRG server [138] and they were manually added into the input file of SHELXL-97.

3.3.4 Validation and quality of the structures

The final quality of the structures was assessed by MOLPROBITY [139], PROCHECK [140] and the various validation tools in COOT. The programme CONTACT was used through the CCP4i to calculate the various types of contacts in the structures. The programme BAVERAGE in CCP4 was used to calculate the average B-factor values for the main chain, side-chain, ligands and the waters.

Structural superposition was carried out by SSM [31] , RMSDs calculated for the C-alphas and the structures were visualized in COOT. Multiple sequence alignment was performed by ClustalW [141], and secondary structure assignment was performed by DSSP [142].

3.4 Presentation

All the schematic protein structure representations were produced with PyMol (http://www.pymol.org). Multiple sequence alignment output from ClustalW was formatted into a coloured postscript file using ESPript [143].

Table 3. Data collection and refinement statistics.

	GST		HpA		
Data collection and processing	GSH	Nb-GSH	In-house	Cryogenic	Room-temp
Wavelength (Å)	0.8088	0.8088	1.5418	0.8081	0.8123
Resolution (Å)	100-2.7 (2.75.2.70)	70.71-1.75 (1.78-1.75)	2.6	99.0-1.4 (1.42-1.40)	99.0-1.8 (1.83-1.80)
Angle Δφ (°)	0.5	0.5	1.5	0.5	0.5
No of images	250	250	100	400	300
Beamline	DESY-X13	DESY-X11	-	DESY-X13	DESY-X13
Cryoprotectant (%)	20	20	25	25	-
Space group	$P6_1$	$P4_12_12$	$I222$	$I222$	$I222$
Unit-cell parameters (Å)	a=b=136.2, c=90.7	a=b=91.4, c=111.9	a=63.6, b=94.8, c=100.3	a=63.6, b=94.8, c=100.3	a=64.9, b=96.4, c=101.9
Completeness (%)	99.0 (100.0)	99.0 (100.0)	97.5 (93.4)	99.7 (99.1)	99.9 (99.4)
$I/\sigma(I)$	28.9 (3.5)	40.1 (4.1)	12.2 (2.4)	22.8 (7.1)	24.8 (3.5)
$R_{merge\ (\%)}$	6.8 (56.3)	5 (52.2)	13.4 (42.3)	9.6 (27.2)	7.2 (50.2)
No. of protein molecules/asymmetric unit	2	2	1	1	1
Matthews coefficient ($Å^3\ Da^{-1}$)	4.9	2.3	2.1	2.1	2.1
Refinement					
Resolution range (Å)	59.0-2.7	70.71-1.75		20.0-1.40	70.0-1.80
R_{cryst}/R_{free} (%)	18.9 /24.1	19.4 / 24.3		13.1/16.9	15.1/18.5
Protein atoms	3656	4243		2531	2428
Water molecules	100	479		391	168
RMSD from ideality					
Bond lengths (Å)	0.015	0.015		0.012	0.014
Bond angles (°)	1.90	1.5		2.52	1.32
PBD code	3fhs	2vo4		2wlt	2wt4

4 SUMMARY OF RESULTS AND DISCUSSION

4.1 Structural aspects of GmGSTU4-4 complexes (Paper II and III)

GmGSTU4-4 displays the characteristic GST fold. The protein is functional as a dimer (Fig. 12) similarly to all the cytosolic GSTs that belong to Tau and Phi classes. The two subunits exhibit only minor structural differences. Salt-bridges, hydrogen bonds and hydrophobic interactions are the three types of interactions involved in the subunit-subunit interface. The dimer adopts a globular shape and each subunit folds to form two spatially distinct domains: a small N-terminal α/β domain (1-77 residues) and a larger C-terminal α-helical domain (89-219 residues) (Fig. 13). A large cleft formed in the centre of the dimer is unique to GSTs. The presence of a large inverted L-shaped active site is also typical to Tau GSTs whereas Phi class GSTs have a large open cavity [144]. One molecule of the ligand was unambiguously observed in each subunit of the complexes.

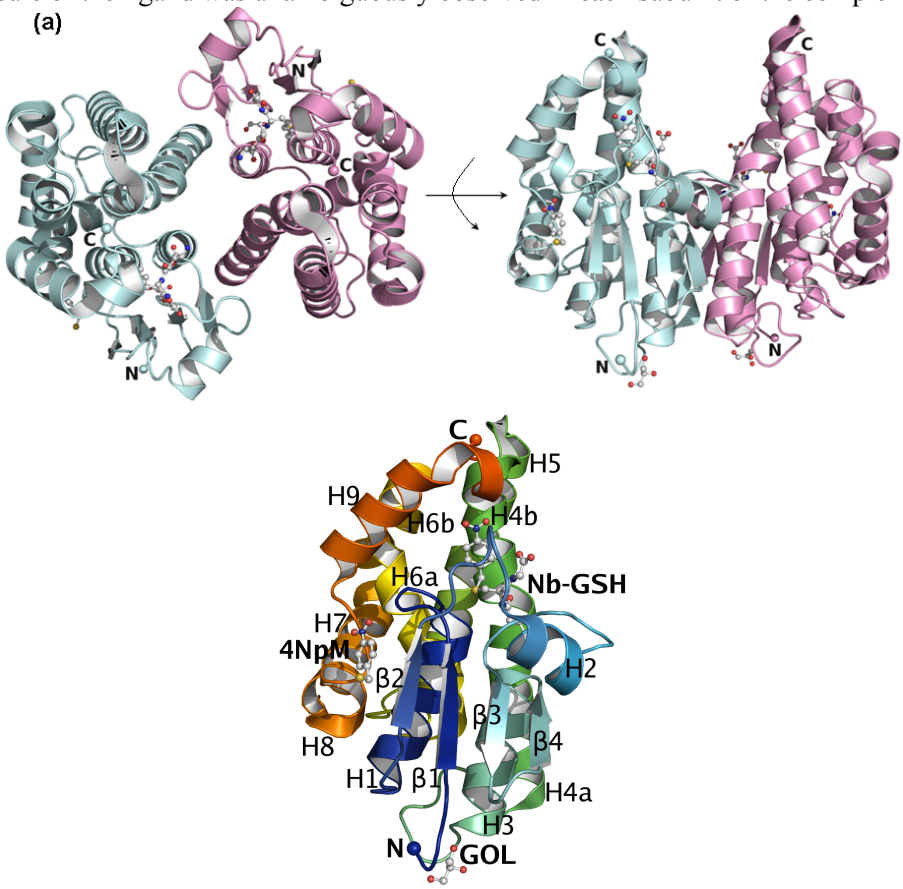

Figure 12. (**a**-left). Cartoon diagram of dimeric GmGSTU4-4 (PDB id: 2vo4) where monomer A is coloured in cyan and monomer B in magenta. (**a**-right) The dimer after 90° rotation. (**b**) Cartoon representation of the monomer. The colouring scheme is from blue (N-terminus) to red (C-terminus) and the ligandsS-(p-nitrobenzyl)-glutathione (Nb-GSH), (4-nitrophenyl) methanethiol (NpM) and glycerol (GOL) are shown in ball and stick representation and coloured according to atom types.

4.1.1 Glutathione-binding site (G-site)

The N-terminal domain binds GSH in a topologically conserved location known as the G-site. The G-site is formed in the beginning of H1, H2 and H3-helices. The Tau class GSTs along with mammalian theta and insect delta use a catalytic serine hydroxyl to activate GSH during catalysis [55]. The hydroxyl group of the serine acts as a hydrogen donor to the thiol group of GSH leading to the formation and subsequent stabilization of the highly reactive thiolate anion which is the target for nucleophilic attack of an electrophilic substrate. The interactions of the G-site in the GSH bound complex are:

- The γ-Glu moiety of GSH points downward to an internal cavity and forms hydrogen bonds with Glu66, Ser67 and Wat250.
- The cysteinyl moiety of GSH is involved in hydrogen bonding with the peptide bond of Ile54.
- The –SH group is involved in water-mediated hydrogen bonding with Lys40 and in weak contacts with the side-chain of Lys53 as well.
- The glycyl moiety of GSH hydrogen bonds with the active site Ser13.

Interestingly, GSH is bound in a different conformation in each subunit of the GmGSTU4-4-GSH complex (Fig. 13). Details about the active site interactions in the individual subunits are as follows:

4.1.1.1 GmGSTU4-4-GSH-Subunit A

Apart from the aforementioned interactions at the active site, the γ-Glu carboxyl group undergoes a water-mediated hydrogen bond with Asp103. The glycyl moiety of GSH in this subunit is located in a more positive electrostatic potential area and is stabilized by a hydrogen bond formed with the side-chain of Tyr107 (2.81 Å). No hydrogen bond is seen between the hydroxyl group of Tyr107 and guanidine group of Arg111. The interaction between the two is important for the subsequent reorientation of GSH to its correct position for catalysis (more details about the binding mechanism are mentioned under section 4.1.3). The –SH group of the cysteine residue of GSH is accessible to the bulk solvent while pointing toward the H-site. The carboxyl group of the glycyl moiety also establishes weak contacts with Phe15 (3.52 Å) and also forms a hydrogen-bond with the catalytic Ser13 (3.45 Å) (Fig. 13). Therefore, the enzyme forms a complex with the ionized form of GSH in the A subunit. The GSH interacts with the enzyme in such a way to form a catalytically competent complex.

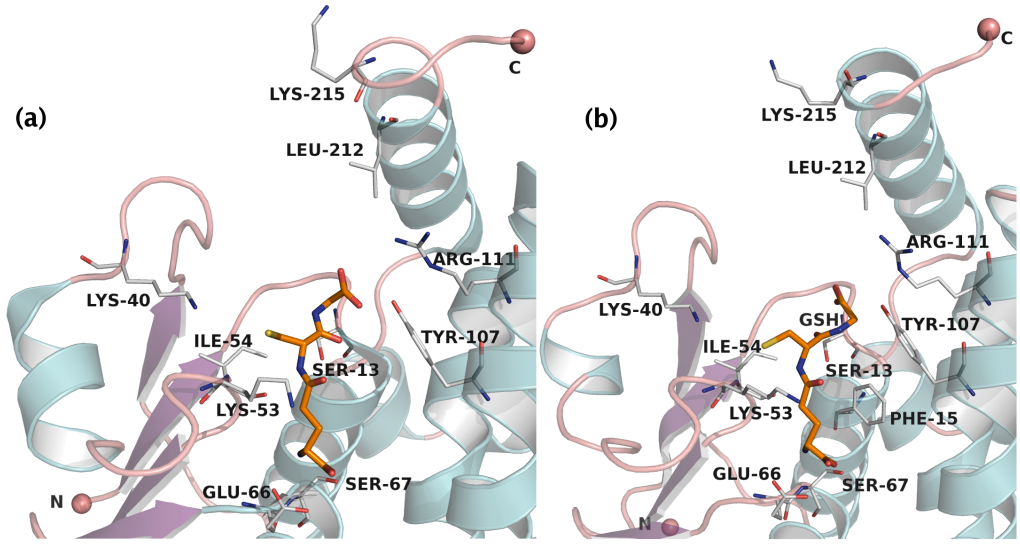

Figure 13. Cartoon representation of the GmGSTU4-4-GSH G-site in subunit A **(a)** and subunit B **(b)**. All the active site residues and GSH are shown in stick representation, coloured according to atom type and labelled.

4.1.1.2 GmGSTU4-4-GSH-Subunit B

While the interactions at the γ-Glu moiety are similar to those of A-subunit, significant differences are observed in the interaction patterns of cysteinyl and glycyl moieties due to their respective conformational variabilities. The –SH group of the cysteinyl moiety makes weak contacts with Lys53, and fails to interact with Lys40 due to a change in the conformation of the –SH reacting group. The glycyl moiety adopts a different conformation by positioning itself away from the H-site and Tyr107 and towards an unfavourable hydrophobic environment formed by Phe10, Pro12, Leu37, Trp163 and Phe208 (Fig. 13). An important feature again is a missing hydrogen bond between Tyr107 and Arg111 owing to a conformational change of the latter pointing away from the active site. This interaction is necessary for the correct positioning of the xenobiotic substrate. These differences might explain the variations in the ionic states of the glycyl moiety in both subunits and further support the possibility of different ionization states of glycine carboxylate. The conformation of the –SH group of GSH in the B subunit probably does not play a role as a nucleophile and, therefore is unable to produce a catalytically competent complex. As a result, GSH binds in a productive (ionised form) mode in subunit A and unproductive (non-ionised form) mode in subunit B.

Two possible explanations could be given for the unproductive binding of GSH in the B subunit: either to prevent the oxidation of the GSH-SH group under oxidative stress conditions or to deliver the bound GSH to specific receptors or cellular compartments by performing a non-catalytic function such as glutathionylation.

4.1.1.3 GmGSTU4-4-Nb-GSH complex

The location of the GSH moiety of the bound Nb-GSH inhibitor is similar to that found in the GmGSTU4-4-GSH complex. The γ-Glu moiety of GSH forms hydrogen bonds with Glu66 and Ser67 and makes weak contacts with Pro55 and Phe15. The amino nitrogen of the cycteinyl moiety forms a hydrogen bond with the peptide bond of Ile54 (2.77 Å). The –sulphur atom of the cysteinyl moiety makes a hydrogen bond with the hydroxyl group of Ser13 (3.24 Å) that facilitates the formation of the thiolate anion. The glycyl moiety of the substrate participates in hydrogen bonds with the side-chain Lys40 and two water-mediated hydrogen bonds with Lys215. The glycyl N and carboxylate are also within hydrogen bonding distances with Wat370 that is further stabilized by Lys53. Asp103 forms a water-mediated hydrogen bond with the Lys104 side-chain from the adjacent subunit contributing to the subunit interface and spatial organization of the dimer.

Although the overall structure of the N-terminal domain is mostly similar (RMSD of 0.18 Å) in the GSH and Nb-GSH complexes, two striking differences have been observed at the C-terminal domain (RMSD of 1.45 Å). These differences are located at the upper part of α-helix α4 (Trp114-Glu120) and the C-terminal domain (Lys214-Glu219) (Fig.14). These differences cannot be attributed to crystal lattice contacts because they are not involved in any interactions with symmetry-related molecules.

Furthermore, structural comparison between the GSH and Nb-GSH complexes via superposition revealed significant differences in the G-site. These differences affect the hydrogen-bonding and electrostatic interaction pattern of GSH with the enzyme. More specifically:

- The glycyl-carboxylate of the Nb-GSH complex is located in a polar environment and is therefore able to form ionic and hydrogen bonds with the ε-amino group side-chain of Lys40 and two water-mediated hydrogen bonds with the side chain of Lys215. The latter interaction is absent in the GSH complex as the α-helix α7 hosting Lys215 exists in a different conformation and is separated by a distance of (~ 15 Å).
- The hydroxyl group of Tyr107 points towards the benzyl ring of the bound substrate. Consequently, an on-face hydrogen bond is formed between the side-chain hydoxyl of Tyr107 and the π-electron cloud of the benzyl group of Nb-GSH. This interaction helps in stabilizing the substrate in its productive orientation. In the GSH-bound structure, the interactions are different in both subunits. In the A subunit, the hydroxyl group of Tyr107 makes a hydrogen bond (2.8 Å) with the glycyl moiety of the bound GSH, pointing towards possible protonation of the hydroxyl group. The absence of a positively charged group further supports the above. In the B-subunit, a similar interaction is absent because the glycyl moiety adopts a different conformation turning away from Tyr107.

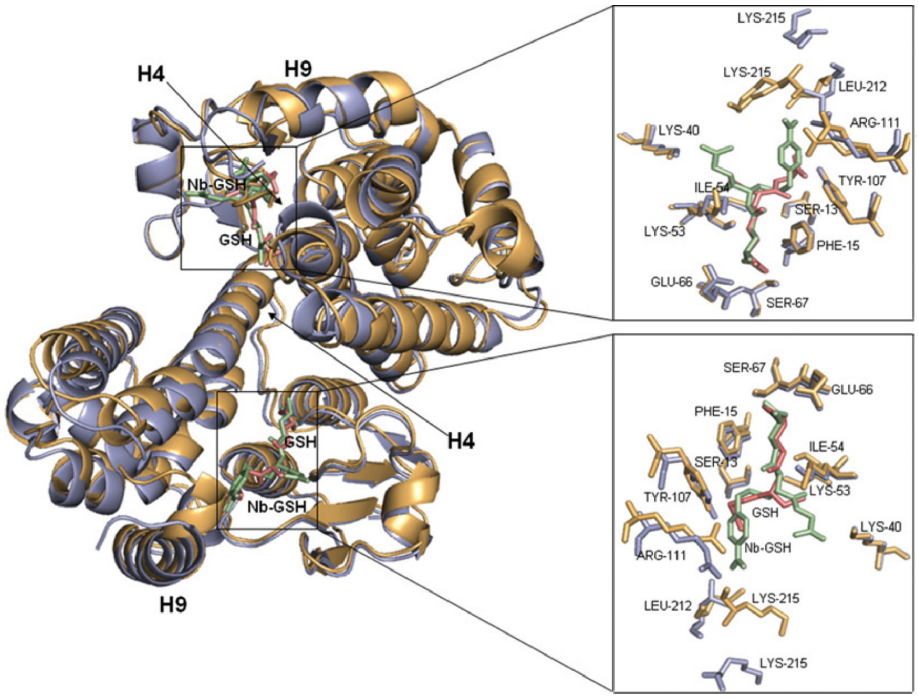

Figure 14. Superposition of GmGSTU4-4-Nb-GSH structure (light orange) onto GmGSTU4-4-GSH (light blue). Ligands (Nb-GSH pale green and GSH salmon) and selected active site residues are represented as sticks. α-Helices H4 and H9 are labelled. This figure was originally published in Biochemical Journal [145].

4.1.2 Hydrophobic substrate-binding site (H-site)

The H-site of GmGSTU4-4 is located next to the G-site and is formed by residues from the C-terminus. The C-terminal domain of the GSTs is found to exhibit a low degree of sequence identity leading to a higher degree of structural plasticity. The H-site is hydrophobic and determines the substrate specificity for hydrophobic substrates. The hydrophobic residues contributing to the H-site of G*m*GSTU4-4-Nb-GSH are: α-helices H4a (Tyr107, Arg111), H6 (Trp163), H9 (Phe208, Leu212, Lys215 and Leu216), and Phe10, and Leu37 from the N-terminal domain. All the residues are oriented towards the centre of the active site and they are not conserved among other classes. This suggests that the size, shape, and binding characteristics of the H-site modulate substrate recognition. The presence of the 4-nitrobenzyl moiety of the bound substrate is directionally towards the bulk solvent. It is bound in a hydrophobic cleft lined by Tyr107 and Trp163 on one side and Phe10, Phe208 and Leu212 on the other (Fig. 14). This could be the reason for the high activity of the enzyme towards hydrophobic substrates (Fig. 2). The nitro-group of the ligand is at a distance of ~ 4 Å from the side-chain of Lys215 and Leu212. Lys215 is not conserved among the Tau class of GSTs and is located in the solvent exposed end of the cleft with its side-chain acting as a lid over the entrance of the active site.

4.1.2.1 Comparison of the H-site between the two complexes

The comparison of the GmGSTU4-4-GSH and Nb-GSH complexes revealed a significant difference in the H-site with respect to the positioning of Arg111 and Tyr107. The guanidine group of Arg111 in the GSH complex has moved 2.3 Å away from the hydroxyl group of Tyr107 resulting in a separation of ~ 5 Å between the two residues. In contrast, in the Nb-GSH complex the interacting group of Arg111 has moved inwards and at a hydrogen bonding distance (2.7 Å) from Tyr107 (Fig. 15).

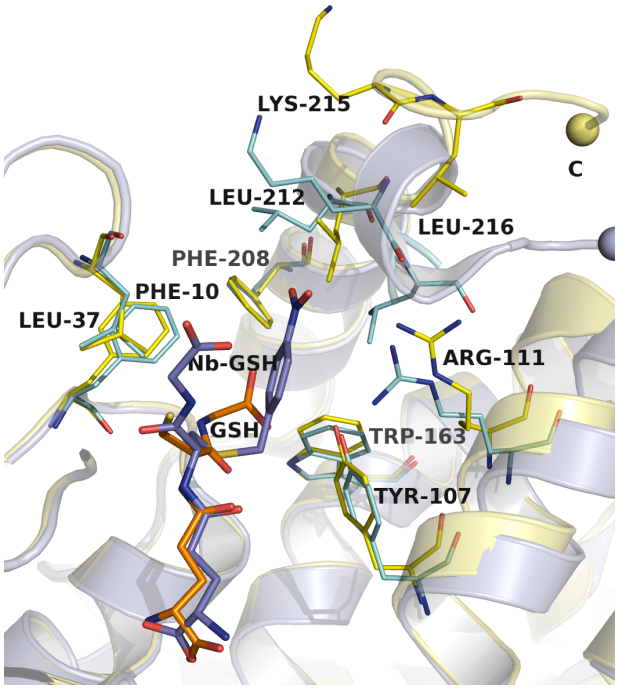

Figure 15. Superposition of GmGSTU4-4-GSH (pale yellow) and GmGSTU4-4-Nb-GSH (light blue) monomer complexes. H-site residues, GSH and Nb-GSH are labelled.

4.1.3 The mechanism of GSH binding

Taking into account the similar binding pattern of the γ-Glu moiety of GSH in both complexes, a mechanism of GSH binding can be described as follows:

- Initially GSH γ-Glu binds followed by the filling of the H-site by the xenobiotic substrate.
- A hydrogen bond is formed between Arg111 and Tyr107.
- Arg111 moves to a new position and the loss of hydrogen bond between Tyr107 and the glycyl oxygen of GSH relocates GSH to an appropriate position for catalysis.
- The xenobiotic ligand is stabilized in the H-site as a result of the Tyr107-Arg111 interactions combined with large conformational changes in the upper part of α-helix H4 (W^{114}TSKGEE^{120}) and the C-terminal residues (K^{214}KLGIE^{219}).

- In the GmGSTU4-4-Nb-GSH complex, the active site is partially blocked by the positioning of the C-terminus as a lid over the top of the N-terminal domain. In contrast, the C-terminus adopts a different conformation and folds away from the entrance of the active site in GmGSTU4-4-GSH complex.

4.1.4 Ligand-binding site (L-site)

One molecule of (4-nitrophenyl) methanethiol was identified in each subunit. The source of the compound could be either some degradation of Nb-GSH, or a by-product during chemical synthesis of Nb-GSH. This compound was found bound in a hydrophobic pocket formed by Trp11, Arg20, Tyr30, Tyr32, Leu199 and Pro200 on the surface of the protein (Fig. 16). The conserved nature of the main binding residues (Trp11, Arg20, Tyr30 and Tyr32) among Tau GST members suggests that this newly identified binding site may be of biological significance and involved in the transfer and delivery of bound ligands to specific protein receptors.

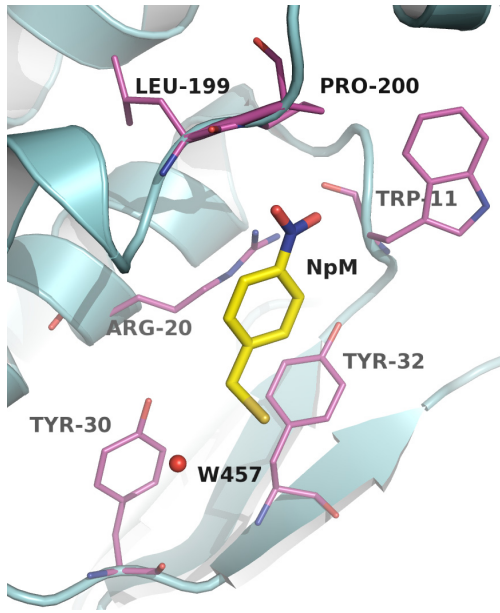

Figure 16. L-site details of the GmGSTU4-4-Nb-GSH complex. (4-nitrophenyl) methanethiol (NpM) and the residues involved in interactions are labelled.

4.2 Structural studies of *H. pylori* L-asparginase (Paper I and IV)

4.2.1 Quality of the HpA structure

HpA structure was refined with anisotropic B-factors to an R_{cryst} of 12.6% for all the 58995 reflections and an R_{free} of 16.9% for 2939 reflections (5% of the total reflections). The final model displays good overall stereochemistry although the first four residues at the N-terminus, residues 22 and 23 could not be modelled due to lack

of sufficient electron density. Residues 21, 24-45 (flexible loop), and 211-216 were refined with 0.65 occupancy owing to their poor density. 99.7% of the non-Gly and non-Pro residues were in the most favoured regions of the Ramachandran plot. Thr204 was identified in the disallowed region that may be due to its strained conformation in spite of the good electron density. Sixteen residues were modelled in alternative conformations.

4.2.2 Description of the structure

The crystals belong to the *I*222 space group. The Matthews coefficient, V_M, [146, 147] of 2.27 $Å^3$ Da^{-1} corresponds to a solvent content of ~ 47% and the presence of one molecule in the asymmetric unit. This is contrary to the presence of non-crystallographic homotetramers in other type-II bacterial L-asparaginases. Another bacterial L-asparaginase that crystallizes as a monomer in the asymmetric unit is that from *Acinetobacter glutaminasificans*, where the active tetramer is generated by crystal symmetry operations [148].

The structure of HpA is characterized by an α/β fold. The monomer consists of 327 amino acids that form 9 α-helices, 14 β-strands and 6 3_{10} helices. The monomer is divided into a large N-terminal domain and a small C-terminal domain connected by a linker of ~ 26 residues. A left-handed crossover between the β4 and β5 strands (residues 119-153) is observed in HpA as in all other L-asparaginases.

4.2.3 Insights into the L-Asp binding site

A strong electron density corresponding to L-Asp was observed at the active site between the N- and C-terminal domains of symmetry-related subunits. Since L-Asp was not added during crystallization, its presence can be explained as an impurity during purification process. Apart from HpA, the structures of L-asparaginases with bound L-Asp are those from *E. coli* [116] and *Erwinia carotovora* [149]. The active site is formed by a flexible part and a rigid part. The flexible part of the active site (19-46) is responsible for controlling the access to the binding site and hosts the catalytically important Thr16, Ser31 and Tyr29. The rigid part is formed by residues between the first and the third parallel β-strands of the N-terminal domain (Ser62, Gln63, Thr95 and Asp96) and by the residues from the loop of the C-terminal domain of the adjacent monomer [101] (Asn255, Glu289). The residues from the rigid part are responsible for the substrate binding (active site residues; Fig 4 Paper IV). The interaction of Ser31 with L-Asp in HpA is noteworthy, as the corresponding residues in EcAII (Val) and in WsA, EwA and ErA (Ala) rule out the possibility of a hydrogen bond formation due to the absence of a suitable side-chain. HpA Gln63 is conserved in WsA, and EcAII whilst is replaced by Gln in EwA, ErA and PgA. Tyr29, another important residue of the active site flexible loop, is characterized by good electron density, suggesting some stabilization upon substrate binding. Tyr29 is also essential for the loop closure and catalysis in EcAII (Fig. 17) [124, 125]. The rigid part of the active site hosts three residues: Asn255, Glu289 and Gln63. Asn255 is conserved in

EcAII and WsA, but is replaced by Ser in EwA, ErA and PgA. HpA Glu289 corresponds to Glu in EcAII whereas Asp replaces it in ErA and EwA (Multiple sequence alignment; Fig. 2 Paper IV).

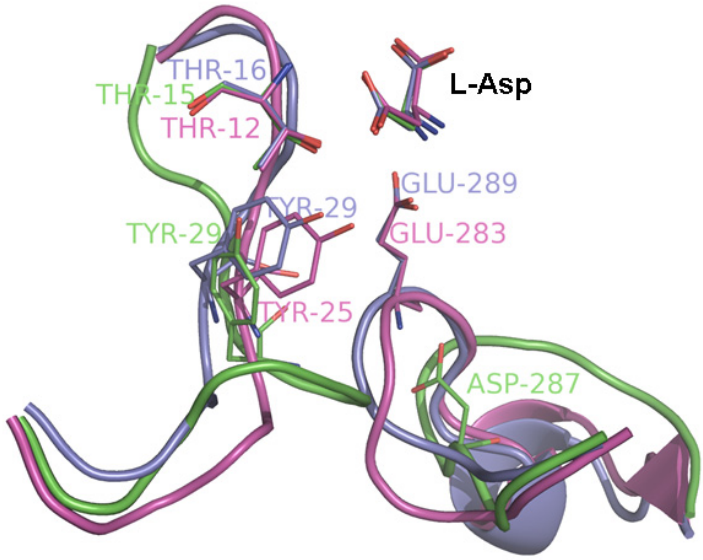

Figure 17. Close-up view of the active site flexible loops. HpA (PDB id: 2wlt [150]), EwA (PDB id: 2gvn [149]) and EcAII (PDB id: 3eca [116]) are coloured in blue, green and magenta, respectively. L-Asp is labelled. Reproduced with permission of the International Union of Crystallography (http://journals.iucr.org/).

4.2.4 Room temperature HpA structure

Although cryogenic techniques reduce radiation damage, they might also introduce structural artefacts directly as a result of temperature effects (e.g. decrease in unit-cell volume, changes in molecular packing and perturbation of local structure) or indirectly from addition of cryoprotectants and temperature-induced pH changes. Thus, high-resolution cryogenic structures may exhibit structural deviations from the room temperature structures. These differences are more extensive on the surface compared to the core of protein [151].

A room temperature structure to 1.8 Å was, therefore, solved for HpA to acquire information about possible temperature-induced changes, especially the position of the flexible loop. Inspection of the electron density maps showed that the position of the loop in both structures is the same. A larger part of the flexible loop (22-35) could not be modelled in the room temperature structure due to lack of electron density (Fig. 18).

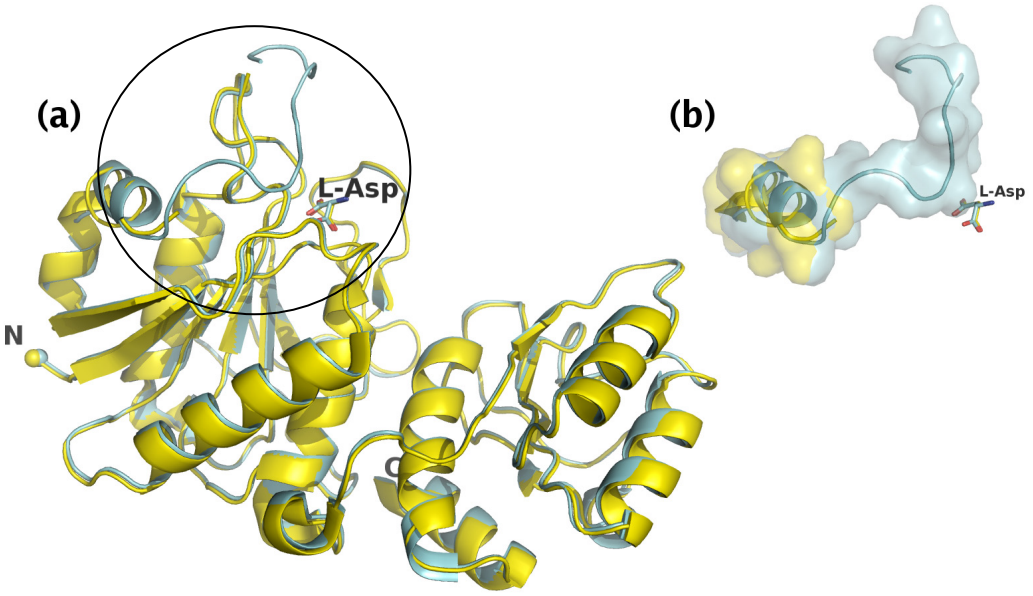

Figure 18. **(a)** Superposition of the cryogenic (PDB id: 2wlt; cyan) and room temperature (PDB id: 2wt4; yellow) structures with the active site flexible loop marked in a circle. L-Asp in both the structures is shown in stick representation and coloured according to atom type. **(b)** The active site flexible loops of the two superposed structures in cartoon and surface representations.

An interesting observation was made for Met197 whose sulphur atom alone is seen in two conformations with lack of electron density for the methyl group. These changes are probably induced by radiation damage.

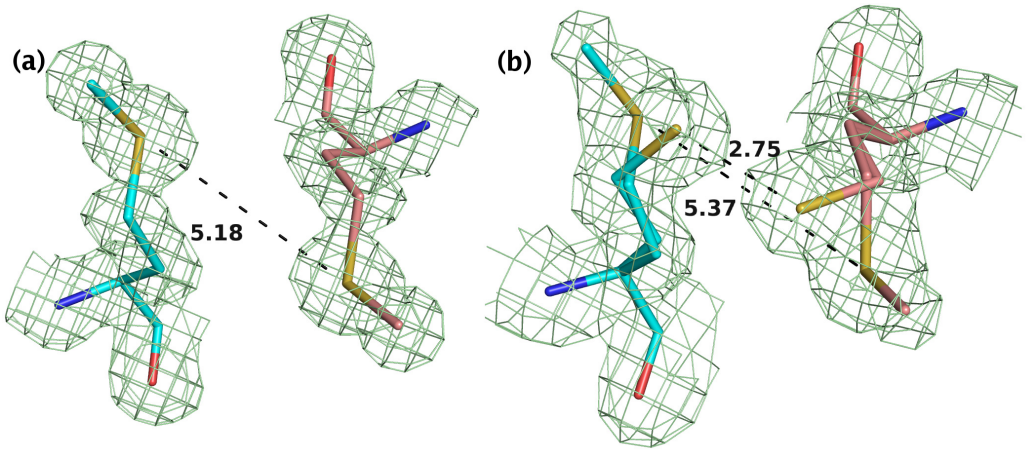

Figure 19. 2Fo-Fc electron density contoured to 1σ for Met197 in the **(a)** cryogenic structure (PDB id: 2wlt); and **(b)** room temperature structure (PDB id: 2wt4). Met197 is coloured according to atom type and the distances between the sulphur atoms are measured and shown as dashed lines.

Met197 is at a cell symmetry axis and the sulphur atom from the alternative conformation is located at 2.75 Å distance from its symmetry-related counterpart. This feature is absent in the cryogenic structure (Fig. 19).

4.2.5 Implications for CCUG-17874 L-asparaginase

A pair-wise sequence alignment between the two sequences (HpA and CCUG-17874 L-asparaginases) showed differences with respect to four residues from the flexible loop (Val22Ala, Asp23Ser, Leu26Ser and Gly27Asp) and three residues at the interface (Gly229Ser, Gly284Glu and Val285Ile) (Fig. 20). However, the residues involved in the interactions with L-Asp are conserved suggesting an agreement between their kinetic and structural properties.

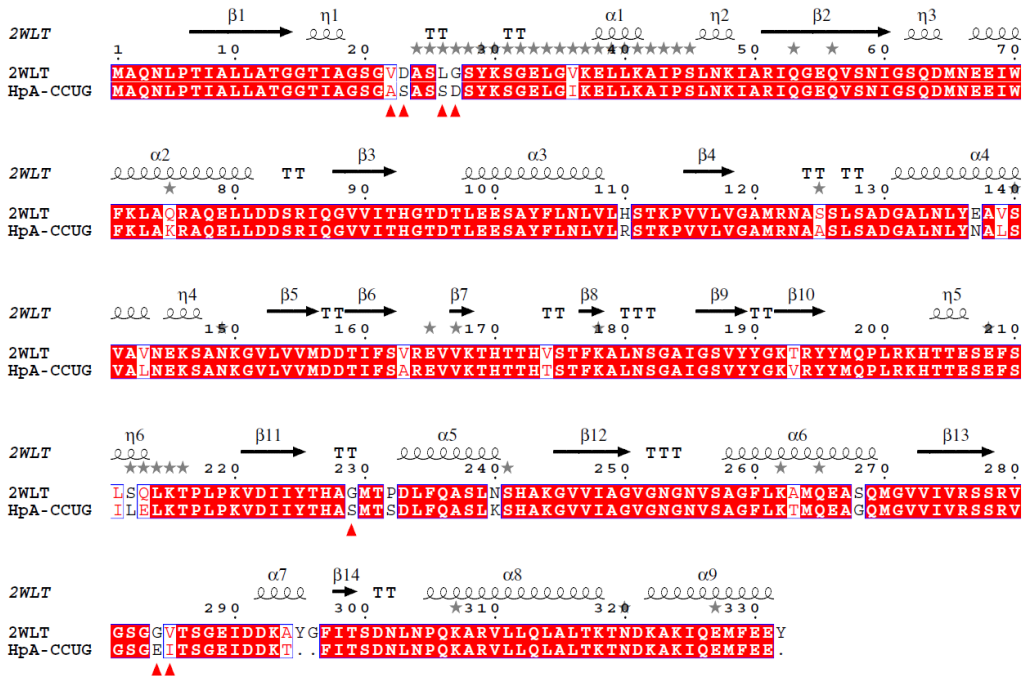

Figure 20. Sequence alignment between the *Helicobacter pylori* J99 (PDB id: 2wlt) and CCUG 17874 strain (UniProt Sequence ID: B6ZCD8). The variable residues from the flexible loop and the interface are marked.

5 CONCLUSIONS AND FUTURE PERSPECTIVES

The presented work has led to the following conclusions:

1. GmGSTU4-4-GSH complex:
   - The conformation of GSH when it binds to a Tau class GST was resolved.
   - GSH binds in two different ionized states: ionized and non-ionized.
   - Tyr107 plays a key role in catalysis.
   - A partially disabled active site may operate in plant GST enzymes.
2. GmGSTU4-4-Nb-GSH complex:
   - Ser13 at the active site stabilizes the thiolate anion of GSH and is also responsible for enhancing its nucleophilicity.
   - Tyr107 and Arg111 together contribute significantly to catalysis.
   - A novel hydrophobic binding site (L-site) formed by conserved residues was identified on the surface of the protein. This site may have a role in the delivery of bound ligands.
   - Structural comparison with the GmGSTU4-4-GSH complex has revealed significant differences in the hydrogen bonding and the electrostatic interaction pattern in the G-site.
3. HpA:
   - The crystal structure of HpA was solved at 1.4-Å resolution, one of the highest among the available L-asparaginase crystal structures.
   - The well-defined position of Ty29 suggests initial stages of flexible loop stabilization.
   - The presence of Ser31 from the flexible loop is unique to HpA L-asparaginase and presents a good target for mutagenesis studies.
   - The active site in HpA and EcAII is more restricted compared to that of ErA. The position of HpA Glu289 suggests similar active site architecture with EcAII. The close proximity of HpA Glu289-Asn255-Gln63 may contribute to higher specificity by excluding large amino acids like glutamine from entering the binding site.

The presented results on the GmGSTU4-4 will help in a rational design of more efficient GSTs that could confer better tolerance to a larger spectrum of xenobiotic compounds as well as the development of new and safer herbicides. Work on HpA could form the basis for the design of chimeric enzymes with desirable features for therapeutic purposes.

6 ACKNOWLEDGEMENTS

This study was carried out in the Centre for Biotechnology, Turku, University of Turku and Åbo Akademi University during the period 2007-2010.

I would like to express my sincere thanks to my supervisor, Docent Dr Tassos Papageorgiou, for giving me the chance to explore the field of protein crystallography. I thank him for his strong cooperation throughout the period of my research. I am indebted for all the guidance that was extended in the various experimental stages of my study, and most importantly for scientific writing. Last but not least, I thank him for providing me with the courage that helped me to stay focussed during the most difficult and final stages of my thesis.

I would like to express my thanks to Prof. Riitta Lahesmaa, director of the Centre, for providing excellent facilities and a friendly atmosphere to carry out my study. I take this opportunity to thank Prof. Jyrki Heino for his valuable advice and kindness.

I am greatly obliged to my reviewers Dr. Petri Kursula and Dr. Ester Boix for their critical and constructive comments which helped me to improve my thesis.

My thanks go to my collaborators, Nikolaos E. Labrou for providing us with purified GST, and Julya Krasotkina for providing constructs to express *Helicobacter pylori* L-asparaginase.

I owe my deepest heart-felt thanks to my fellow graduate student Teemu Haikarainen for being such a great colleague and friend at work. I thank him for all the scintillating conversations in the otherwise dark graphics room about the various practical and technical aspects of the subject. I wish to thank him for his presence in all the good and bad times of my study that helped me to enjoy a very healthy atmosphere at work. I would like to thank Heli Havukainen for all the warmth that was greatly required during the initial stages of my study in Turku. I wish to thank Bhanu, Sachin, Abdi, Bishwa and all the past and present members of the group for being the wonderful people that they are.

I wish to thank the secretarial staff at CBT, Aila Jasmavaara, Eva Hirvensalo, and Sirkku Grönroos, for helping me with a warm smile whenever necessary. I thank the technical staff, especially Petri Vahakoski and Mårten Hedman, for providing excellent support with the Linux and Windows workstations.

My sincere thanks go to my parents who are responsible for sowing the seeds of inquisitiveness and enthusiasm towards science in me during the early years of my life. I thank my brother Hemanth and his wife Swarna for making their presence felt through frequent phone calls. I wish to thank my parents-in-law for their prayers and blessings. I take this opportunity to thank all my friends and their families in Finland for the happy and warm evening dinners and friendly chats over coffee. I owe my thanks to my Indian friends for organizing all the festivals which made me feel at home over the period of my study.

I thank my husband Suresh for keeping me in the warmest place of his heart which helped me cope with the ups and downs of my study and the Finnish winters. Most of

all I wish to thank him for showing me the positive perspective of life and above all for his true love. My daughter Lasya Dyuti shares a major contribution to the success of my research by providing a soothing effect with her laughter and smiles.

I wish to offer my sincerest thanks and prayers to my spiritual Master Shri Shri Shri Sharvari Guru garu for giving me all the positive spiritual strength required to pursue life and research. I wish to thank all the Hindu gods and goddesses for their blessings and all my spiritual friends for sharing their wonderful thoughts and experiences.

This work was funded by the Centre for International Mobility in Finland, Sigrid Jusélius Foundation, and the Academy of Finland.

Turku, March 2011

Prathusha

7 REFERENCES

1. Booth J, Boyland E & Sims P (1961) An enzyme from rat liver catalysing conjugations with glutathione. *Biochem J* **79**, 516-524.
2. Frear DS & Swanson HR (1970) Biosynthesis of S-(4-ethylamino-6-isopropylamino- 2-s-triazino) glutathione: Partial purification and properties of a glutathione S-transferase from corn. *Phytochemistry* **9**, 2123-2132.
3. Wilce MC & Parker MW (1994) Structure and function of glutathione S-transferases. *Biochim Biophys Acta* **1205**, 1-18.
4. Sheehan D, Meade G, Foley VM & Dowd CA (2001) Structure, function and evolution of glutathione transferases: implications for classification of non-mammalian members of an ancient enzyme superfamily. *Biochem J* **360**, 1-16.
5. Armstrong RN (1997) Structure, catalytic mechanism, and evolution of the glutathione transferases. *Chem Res Toxicol* **10**, 2-18.
6. Schröder P & Collins C (2002) Conjugating enzymes involved in xenobiotic metabolism of organic xenobiotics in plants. *Int J Phytorem* **4**, 247-265.
7. Schröder P (2006) Enzymes transferring biomolecules to organic foreign compounds: A role for glucosyltransferase and glutathione S-transferase in phytoremediation. *Phytorem Rhizorem*, 133-142.
8. Shimabukuro RH, Walsh WC & Hoerauf RA (1979) Metabolism and selectivity of diclofop-methyl in wild oat and wheat. *J Agric Food Chem* **27**, 615-623.
9. Sandermann H, Jr. (1992) Plant metabolism of xenobiotics. *Trends Biochem Sci* **17**, 82-84.
10. Barrett M (1995) Metabolism of herbicides by cytochrome P450 in corn. *Drug Metabol Drug Interact* **12**, 299-315.
11. Frear DS (1995) Wheat microsomal cytochrome P450 monooxygenases: characterization and importance in the metabolic detoxification and selectivity of wheat herbicides. *Drug Metabol Drug Interact* **12**, 329-357.
12. Guengerich FP (1992) Metabolic activation of carcinogens. *Pharmacol Ther* **54**, 17-61.
13. Pamela JH, David D, David JC & Robert E (1996) Glutathione transferase activities and herbicide selectivity in maize and associated weed species. *Pestic Sci* **46**, 267-275.
14. Coleman J, Blake-Kalff M & Davies E (1997) Detoxification of xenobiotics by plants: chemical modification and vacuolar compartmentation. *Trends Plant Sci* **2**, 144-151.
15. Ishikawa T (1992) The ATP-dependent glutathione S-conjugate export pump. *Trends in Biochem Sci* **17**, 463-468.
16. Theodoulou FL (2000) Plant ABC transporters. *Biochim Biophys Acta* **1465**, 79-103.
17. Schmitt R & Sandermann H (1982) Localization of b-D-glucoside conjugates of 2,4-dichlorophenoxyacetic acid in soybean vacuoles. *Naturforschung* **37c**, 772−777.
18. Martinoia E, Grill E, Tommasini R, Kreuz K & Amrhein N (1993) ATP-dependent glutathione S-conjugate 'export' pump in the vacuolar membrane of plants. *Nature* **364**, 247-249.
19. Kreuz K, Tommasini R & Martinoia E (1996) Old enzymes for a new job (herbicide detoxification in plants). *J Plant Physiol* **111**, 349-353.
20. Talalay P, De Long MJ & Prochaska HJ (1988) Identification of a common chemical signal regulating the induction of enzymes that protect against chemical carcinogenesis. *Proc Natl Acad Sci U S A* **85**, 8261-8265.
21. Hayes JD & McLellan LI (1999) Glutathione and glutathione-dependent enzymes represent a co-ordinately regulated defence against oxidative stress. *Free Radic Res* **31**, 273-300.
22. Hayes JD, Flanagan JU & Jowsey IR (2005) Glutathione transferases. *Annu Rev Pharmacol Toxicol* **45**, 51-88.
23. McGonigle B, Keeler S, Lau S, Koeppe M & O'Keefe D (2000) A genomics approach to the comprehensive analysis of the glutathione S-transferase gene family in soybean and maize. *Plant Physiol* **124**, 1105-1120.
24. Ranson H, Collins F & Hemingway J (1998) The role of alternative mRNA splicing in generating heterogeneity within the *Anopheles gambiae* class I glutathione S-transferase family. *Proc Natl Acad Sci U S A* **95**, 14284-14289.

25. Morel F, Rauch C, Petit E, Piton A, Theret N, Coles B & Guillouzo A (2004) Gene and protein characterization of the human glutathione S-transferase kappa and evidence for a peroxisomal localization. *J Biol Chem* **279**, 16246-16253.

26. Mannervik B & Danielson UH (1988) Glutathione transferases--structure and catalytic activity. *CRC Crit Rev Biochem* **23**, 283-337.

27. Soranzo N, Sari Gorla M, Mizzi L, De Toma G & Frova C (2004) Organisation and structural evolution of the rice glutathione S-transferase gene family. *Mol Genet Genomics* **271**, 511-521.

28. Edwards R & Dixon DP (2005) Plant glutathione transferases. *Methods Enzymol* **401**, 169-186.

29. Chronopoulou EG & Labrou NE (2009) Glutathione transferases: emerging multidisciplinary tools in red and green biotechnology. *Recent Pat Biotechnol* **3**, 211-223.

30. Thom R, Cummins I, Dixon DP, Edwards R, Cole DJ & Lapthorn AJ (2002) Structure of a tau class glutathione S-transferase from wheat active in herbicide detoxification. *Biochemistry* **41**, 7008-7020.

31. Krissinel E & Henrick K (2004) Secondary-structure matching (SSM), a new tool for fast protein structure alignment in three dimensions. *Acta Crystallogr D Biol Crystallogr* **60**, 2256-2268.

32. Cameron AD, Sinning I, L'Hermite G, Olin B, Board PG, Mannervik B & Jones TA (1995) Structural analysis of human alpha-class glutathione transferase A1-1 in the apo-form and in complexes with ethacrynic acid and its glutathione conjugate. *Structure* **3**, 717-727.

33. Ji X, Armstrong RN & Gilliland GL (1993) Snapshots along the reaction coordinate of an SNAr reaction catalyzed by glutathione transferase. *Biochemistry* **32**, 12949-12954.

34. Reinemer P, Dirr HW, Ladenstein R, Huber R, Lo Bello M, Federici G & Parker MW (1992) Three-dimensional structure of class pi glutathione S-transferase from human placenta in complex with S-hexylglutathione at 2.8 A resolution. *J Mol Biol* **227**, 214-226.

35. Nishida M, Harada S, Noguchi S, Satow Y, Inoue H & Takahashi K (1998) Three-dimensional structure of *Escherichia coli* glutathione S-transferase complexed with glutathione sulfonate: catalytic roles of Cys10 and His106. *J Mol Biol* **281**, 135-147.

36. Rossjohn J, McKinstry WJ, Oakley AJ, Verger D, Flanagan J, Chelvanayagam G, Tan KL, Board PG & Parker MW (1998) Human theta class glutathione transferase: the crystal structure reveals a sulfate-binding pocket within a buried active site. *Structure* **6**, 309-322.

37. Thom R, Dixon DP, Edwards R, Cole DJ & Lapthorn AJ (2001) The structure of a zeta class glutathione S-transferase from *Arabidopsis thaliana*: characterisation of a GST with novel active-site architecture and a putative role in tyrosine catabolism. *J Mol Biol* **308**, 949-962.

38. Board PG, Coggan M, Chelvanayagam G, Easteal S, Jermiin LS, Schulte GK, Danley DE, Hoth LR, Griffor MC, Kamath AV, et al. (2000) Identification, characterization, and crystal structure of the Omega class glutathione transferases. *J Biol Chem* **275**, 24798-24806.

39. Reinemer P, Prade L, Hof P, Neuefeind T, Huber R, Zettl R, Palme K, Schell J, Koelln I, Bartunik HD, et al. (1996) Three-dimensional structure of glutathione S-transferase from *Arabidopsis thaliana* at 2.2 A resolution: structural characterization of herbicide-conjugating plant glutathione S-transferases and a novel active site architecture. *J Mol Biol* **255**, 289-309.

40. Mueller LA, Goodman CD, Silady RA & Walbot V (2000) AN9, a petunia glutathione S-transferase required for anthocyanin sequestration, is a flavonoid-binding protein. *Plant Physiol* **123**, 1561-1570.

41. Jakobsson PJ, Morgenstern R, Mancini J, Ford-Hutchinson A & Persson B (1999) Common structural features of MAPEG -- a widespread superfamily of membrane associated proteins with highly divergent functions in eicosanoid and glutathione metabolism. *Protein Sci* **8**, 689-692.

42. Smith AP, DeRidder BP, Guo WJ, Seeley EH, Regnier FE & Goldsbrough PB (2004) Proteomic analysis of *Arabidopsis* glutathione S-transferases from benoxacor- and copper-treated seedlings. *J Biol Chem* **279**, 26098-26104.

43. Cho HY & Kong KH (2007) Study on the biochemical characterization of herbicide detoxification enzyme, glutathione S-transferase. *Biofactors* **30**, 281-287.

44. Frova C (2003) The plant glutathione transferase gene family: genomic structure, functions, expression and evolution. *Physiol Plant* **119**, 469-479.

45. Neuefeind T, Huber R, Reinemer P, Knablein J, Prade L, Mann K & Bieseler B (1997) Cloning, sequencing, crystallization and X-ray structure of glutathione S-transferase-III from *Zea mays* var. mutin: a leading enzyme in detoxification of maize herbicides. *J Mol Biol* **274**, 577-587.

46. Loyall L, Uchida K, Braun S, Furuya M & Frohnmeyer H (2000) Glutathione and a UV light-induced glutathione S-transferase are involved in signaling to chalcone synthase in cell cultures. *Plant Cell* **12**, 1939-1950.

47. Kampranis SC, Damianova R, Atallah M, Toby G, Kondi G, Tsichlis PN & Makris AM (2000) A novel plant glutathione S-transferase/peroxidase suppresses Bax lethality in yeast. *J Biol Chem* **275**, 29207-29216.

48. Edwards R, Dixon DP & Walbot V (2000) Plant glutathione S-transferases: enzymes with multiple functions in sickness and in health. *Trends Plant Sci* **5**, 193-198.

49. Frova C (2006) Glutathione transferases in the genomics era: new insights and perspectives. *Biomol Eng* **23**, 149-169.

50. Dixon DP, Lapthorn A & Edwards R (2002) Plant glutathione transferases. *Genome Biol* **3**, 3004.3001-3010.

51. Martin JL (1995) Thioredoxin--a fold for all reasons. *Structure* **3**, 245-250.

52. Qi Y & Grishin NV (2005) Structural classification of thioredoxin-like fold proteins. *Proteins* **58**, 376-388.

53. Allocati N, Casalone E, Masulli M, Ceccarelli I, Carletti E, Parker MW & Ilio CD (1999) Functional analysis of the evolutionarily conserved proline 53 residue in *Proteus mirabilis* glutathione transferase B1-1. *FEBS letters* **445**, 347-350.

54. Thom R, Cummins I, Dixon D, Edwards R, Cole D & Lapthorn A (2002) Structure of a tau class glutathione S-transferase from wheat active in herbicide detoxification. *Biochemistry* **41**, 7008-7020.

55. Prade L, Hof P & Bieseler B (1997) Dimer interface of glutathione S-transferase from *Arabidopsis thaliana*: influence of the G-site architecture on the dimer interface and implications for classification. *Biol Chem* **378**, 317-320.

56. Dirr H, Reinemer P & Huber R (1994) X-ray crystal structures of cytosolic glutathione S-transferases. Implications for protein architecture, substrate recognition and catalytic function. *Eur J Biochem* **220**, 645-661.

57. Hayeshi R, Chinyanga F, Chengedza S & Mukanganyama S (2006) Inhibition of human glutathione transferases by multidrug resistance chemomodulators in vitro. *J Enzyme Inhib Med Chem* **21**, 581-587.

58. Achilonu I, Gildenhuys S, Fisher L, Burke J, Fanucchi S, Sewell BT, Fernandes M & Dirr HW (2010) The role of a topologically conserved isoleucine in glutathione transferase structure, stability and function. *Acta Crystallogr Sect F Struct Biol Cryst Commun* **66**, 776-780.

59. Abhilash PC, Jamil S & Singh N (2009) Transgenic plants for enhanced biodegradation and phytoremediation of organic xenobiotics. *Biotechnol Adv* **27**, 474-488.

60. Salt DE, Smith RD & Raskin I (1998) Phytoremediation. *Annu Rev Plant Physiol Plant Mol Biol* **49**, 643-668.

61. Gerhardt KE, Huang X-D, Glick BR & Greenberg BM (2009) Phytoremediation and rhizoremediation of organic soil contaminants: potential and challenges. *Plant Sci* **176**, 20-30.

62. Glick BR (2003) Phytoremediation: synergistic use of plants and bacteria to clean up the environment. *Biotechnol Adv* **21**, 383-393.

63. Shiota N, Nagasawa A, Sakaki T, Yabusaki Y & Ohkawa H (1994) Herbicide-resistant tobacco plants expressing the fused enzyme between rat cytochrome P4501A1 (CYP1A1) and yeast NADPH-cytochrome P450 oxidoreductase. *Plant Physiol* **106**, 17-23.

64. Lamoureux GL, Shimabukuro RH, Swanson HR & Frear DS (1970) Metabolism of 2-chloro-4-ethylamino-6-isopropylamino-s-triazine (atrazine) in excised sorghum leaf sections. *J Agric Food Chem* **18**, 81-86.

65. Noctor G & Foyer CH (1998) Ascorbate and glutathione: keeping active oxygen under control. *Annu Rev Plant Physiol Plant Mol Biol* **49**, 249-279.

66. Flocco CG, Lindblom SD & Smits EA (2004) Overexpression of enzymes involved in glutathione synthesis enhances tolerance to organic pollutants in *Brassica juncea*. *Int J Phytoremediation* **6**, 289-304.

67. Karavangeli M, Labrou NE, Clonis YD & Tsaftaris A (2005) Development of transgenic tobacco plants overexpressing maize glutathione S-transferase I for chloroacetanilide herbicides phytoremediation. *Biomol Eng* **22**, 121-128.

68. Dixit P, Singh S, Mukherjee PK & Eapen S (2008) Development of transgenic plants with cytochrome P4502E1 gene and glutathione-S-transferase gene for degradation of organic pollutants. *J Biotechnol* **136**, 692-693.

69. Choi JW, Kim YK, Song SY, Lee IH & Lee WH (2003) Optical biosensor consisting of glutathione-S-transferase for detection of captan. *Biosens Bioelectron* **18**, 1461-1466.

70. Hasegawa K, Miwa S, Tajima T, Tsutsumiuchi K, Taniguchi H & Miwa J (2007) A rapid and inexpensive method to screen for common foods that reduce the action of acrylamide, a harmful substance in food. *Toxicol Lett* **175**, 82-88.

71. Martens DA & Bremner JM (1997) Inhibitory effects of fungicides on hydrolysis of urea and nitrification of urea nitrogen in soil. *Pestic Sci* **49**, 344-352.

72. Mao W, Lumsden RD, Lewis JA & Hebbar PK (1998) Seed treatment using pre-infiltration and biocontrol agents to reduce damping-off of corn caused by *Pythium* and *Fusarium*. *Am Phytopathol Soc* **82**, 294-299.

73. Mueller DS, Hartman GL & Pedersen WL (1999) Development of sclerotia and apothecia of *Sclerotinia sclerotiorum* from infected soybean seed and its control by fungicide seed treatment. *Plant Dis* **83**, 1113-1115.

74. Fan KC, Huang YC & Li CH (1995) Radioimmunoassay for plasma glutathione S-transferase-pi and its clinical application in gastrointestinal cancer. *Cancer* **76**, 1363-1367.

75. Covolo L, Placidi D, Gelatti U, Carta A, Scotto Di Carlo A, Lodetti P, Picciche A, Orizio G, Campagna M, Arici C, et al. (2008) Bladder cancer, GSTs, NAT1, NAT2, SULT1A1, XRCC1, XRCC3, XPD genetic polymorphisms and coffee consumption: a case-control study. *Eur J Epidemiol* **23**, 355-362.

76. Oldenburg J, Kraggerud SM, Brydoy M, Cvancarova M, Lothe RA & Fossa SD (2007) Association between long-term neurotoxicities in testicular cancer survivors and polymorphisms in glutathione-s-transferase-P1 and -M1, a retrospective cross sectional study. *J Transl Med* **5**, 70.

77. Sweeney C, Ambrosone CB, Joseph L, Stone A, Hutchins LF, Kadlubar FF & Coles BF (2003) Association between a glutathione S-transferase A1 promoter polymorphism and survival after breast cancer treatment. *Int J Cancer* **103**, 810-814.

78. Habdous M, Vincent-Viry M, Visvikis S & Siest G (2002) Rapid spectrophotometric method for serum glutathione S-transferases activity. *Clin Chim Acta* **326**, 131-142.

79. Li YJ, Scott WK, Zhang L, Lin PI, Oliveira SA, Skelly T, Doraiswamy MP, Welsh-Bohmer KA, Martin ER, Haines JL, et al. (2006) Revealing the role of glutathione S-transferase omega in age-at-onset of Alzheimer and Parkinson diseases. *Neurobiol Aging* **27**, 1087-1093.

80. Townsend DM & Tew KD (2003) The role of glutathione-S-transferase in anti-cancer drug resistance. *Oncogene* **22**, 7369-7375.

81. Filomeni G, Turella P, Dupuis ML, Forini O, Ciriolo MR, Cianfriglia M, Pezzola S, Federici G & Caccuri AM (2008) 6-(7-Nitro-2,1,3-benzoxadiazol-4-ylthio)hexanol, a specific glutathione S-transferase inhibitor, overcomes the multidrug resistance (MDR)-associated protein 1-mediated MDR in small cell lung cancer. *Mol Cancer Ther* **7**, 371-379.

82. Turella P, Filomeni G, Dupuis ML, Ciriolo MR, Molinari A, De Maria F, Tombesi M, Cianfriglia M, Federici G, Ricci G, et al. (2006) A strong glutathione S-transferase inhibitor overcomes the P-glycoprotein-mediated resistance in tumor cells. 6-(7-Nitro-2,1,3-benzoxadiazol-4-ylthio)hexanol (NBDHEX) triggers a caspase-dependent apoptosis in MDR1-expressing leukemia cells. *J Biol Chem* **281**, 23725-23732.

83. Morgan AS, Ciaccio PJ, Tew KD & Kauvar LM (1996) Isozyme-specific glutathione S-transferase inhibitors potentiate drug sensitivity in cultured human tumor cell lines. *Cancer Chemother Pharmacol* **37**, 363-370.

84. Nare B, Smith JM & Prichard RK (1992) Mechanisms of inactivation of *Schistosoma mansoni* and mammalian glutathione S-

transferase activity by the antischistosomal drug oltipraz. *Biochem Pharmacol* **43**, 1345-1351.

85. Liebau E, Eckelt VH, Wildenburg G, Teesdale-Spittle P, Brophy PM, Walter RD & Henkle-Duhrsen K (1997) Structural and functional analysis of a glutathione S-transferase from *Ascaris suum*. *Biochem J* **324 (Pt 2)**, 659-666.

86. Clementi A (1922) Désamidation enzymatique de L'asparagine chez les différentes espéces animales et la signification physio logique de sa presence dans l'organisme. *Arch Physiol Biochem* **19**, 369-398.

87. Broome JD (1961) Evidence that the L-asparaginase activity of guinea pig serum is responsible for its antilymphoma effects. *Nature* **191**, 1114-1115.

88. Kidd JG (1953) Regression of transplanted lymphomas induced in vivo by means of normal guinea pig serum. I. Course of transplanted cancers of various kinds in mice and rats given guinea pig serum, horse serum, or rabbit serum. *J Exp Med* **98**, 565-582.

89. Asselin BL, Ryan D, Frantz CN, Bernal SD, Leavitt P, Sallan SE & Cohen HJ (1989) In vitro and in vivo killing of acute lymphoblastic leukemia cells by L-asparaginase. *Cancer Res* **49**, 4363-4368.

90. Sallan SE, Hitchcock-Bryan S, Gelber R, Cassady JR, Frei E, 3rd & Nathan DG (1983) Influence of intensive asparaginase in the treatment of childhood non-T-cell acute lymphoblastic leukemia. *Cancer Res* **43**, 5601-5607.

91. Tallal L, Tan C, Oettgen H, Wollner N, McCarthy M, Helson L, Burchenal J, Karnofsky D & Murphy ML (1970) E. coli L-asparaginase in the treatment of leukemia and solid tumors in 131 children. *Cancer* **25**, 306-320.

92. Stams WA, den Boer ML, Holleman A, Appel IM, Beverloo HB, van Wering ER, Janka-Schaub GE, Evans WE & Pieters R (2005) Asparagine synthetase expression is linked with L-asparaginase resistance in TEL-AML1-negative but not TEL-AML1-positive pediatric acute lymphoblastic leukemia. *Blood* **105**, 4223-4225.

93. Richards NG & Kilberg MS (2006) Asparagine synthetase chemotherapy. *Annu Rev Biochem* **75**, 629-654.

94. Aslanian AM & Kilberg MS (2001) Multiple adaptive mechanisms affect asparagine synthetase substrate availability in asparaginase-resistant MOLT-4 human leukaemia cells. *Biochem J* **358**, 59-67.

95. Derst C, Henseling J & Rohm KH (1992) Probing the role of threonine and serine residues of *E. coli* asparaginase II by site-specific mutagenesis. *Protein Eng* **5**, 785-789.

96. Carter P & Wells JA (1988) Dissecting the catalytic triad of a serine protease. *Nature* **332**, 564-568.

97. Michalska K & Jaskolski M (2006) Structural aspects of L-asparaginases, their friends and relations. *Acta Biochim Pol* **53**, 627-640.

98. Wriston JC, Jr. (1985) Asparaginase. *Methods Enzymol* **113**, 608-618.

99. Yurek E, Peru D & Wriston JC, Jr. (1983) On the distribution of plasma L-asparaginase. *Experientia* **39**, 383-385.

100. Wriston JC, Jr. & Yellin TO (1973) L-asparaginase: a review. *Adv Enzymol Relat Areas Mol Biol* **39**, 185-248.

101. Aghaiypour K, Wlodawer A & Lubkowski J (2001) Structural basis for the activity and substrate specificity of *Erwinia chrysanthemi* L-asparaginase. *Biochemistry* **40**, 5655-5664.

102. Schwartz JH, Reeves JY & Broome JD (1966) Two L-asparaginases from *E. coli* and their action against tumors. *Proc Natl Acad Sci U S A* **56**, 1516-1519.

103. Ertel IJ, Nesbit ME, Hammond D, Weiner J & Sather H (1979) Effective dose of L-asparaginase for induction of remission in previously treated children with acute lymphocytic leukemia: a report from Childrens Cancer Study Group. *Cancer Res* **39**, 3893-3896.

104. Verma N, Kumar K, Kaur G & Anand S (2007) L-asparaginase: a promising chemotherapeutic agent. *Crit Rev Biotechnol* **27**, 45-62.

105. Ollenschlager G, Roth E, Linkesch W, Jansen S, Simmel A & Modder B (1988) Asparaginase-induced derangements of glutamine metabolism: the pathogenetic basis for some drug-related side-effects. *Eur J Clin Invest* **18**, 512-516.

106. Molineux G (2003) Pegylation: engineering improved biopharmaceuticals for oncology. *Pharmacotherapy* **23**, 3S-8S.

107. Avramis VI, Sencer S, Periclou AP, Sather H, Bostrom BC, Cohen LJ, Ettinger AG, Ettinger LJ, Franklin J, Gaynon PS, et al. (2002) A randomized comparison of native *Escherichia coli* asparaginase and polyethylene glycol conjugated asparaginase for treatment of children with newly diagnosed standard-risk acute lymphoblastic leukemia: a Children's Cancer Group study. *Blood* **99**, 1986-1994.

108. Park YK, Abuchowski A, Davis S & Davis F (1981) Pharmacology of *Escherichia coli*-L-asparaginase polyethylene glycol adduct. *Anticancer Res* **1**, 373-376.

109. Zeidan A, Wang ES & Wetzler M (2009) Pegasparaginase: where do we stand? *Expert Opin Biol Ther* **9**, 111-119.

110. Fu CH & Sakamoto KM (2007) PEG-asparaginase. *Expert Opin Pharmacother* **8**, 1977-1984.

111. Apostolidou E, Swords R, Alvarado Y & Giles FJ (2007) Treatment of acute lymphoblastic leukaemia : a new era. *Drugs* **67**, 2153-2171.

112. Cedar H & Schwartz JH (1967) Localization of the two-L-asparaginases in anaerobically grown *Escherichia coli*. *J Biol Chem* **242**, 3753-3755.

113. Willis RC & Woolfolk CA (1974) Asparagine utilization in *Escherichia coli*. *J Bacteriol* **118**, 231-241.

114. Ho PP, Milikin EB, Bobbitt JL, Grinnan EL, Burck PJ, Frank BH, Boeck LD & Squires RW (1970) Crystalline L-asparaginase from *Escherichia coli* B. I. Purification and chemical characterization. *J Biol Chem* **245**, 3708-3715.

115. Douer D (2008) Is asparaginase a critical component in the treatment of acute lymphoblastic leukemia? *Best Pract Res Clin Haematol* **21**, 647-658.

116. Swain AL, Jaskolski M, Housset D, Rao JK & Wlodawer A (1993) Crystal structure of *Escherichia coli* L-asparaginase, an enzyme used in cancer therapy. *Proc Natl Acad Sci U S A* **90**, 1474-1478.

117. Yun MK, Nourse A, White SW, Rock CO & Heath RJ (2007) Crystal structure and allosteric regulation of the cytoplasmic *Escherichia coli* L-asparaginase I. *J Mol Biol* **369**, 794-811.

118. Lubkowski J, Dauter M, Aghaiypour K, Wlodawer A & Dauter Z (2003) Atomic resolution structure of *Erwinia chrysanthemi* L-asparaginase. *Acta Crystallogr D Biol Crystallogr* **59**, 84-92.

119. Miller M, Rao JK, Wlodawer A & Gribskov MR (1993) A left-handed crossover involved in amidohydrolase catalysis. Crystal structure of *Erwinia chrysanthemi* L-asparaginase with bound L-aspartate. *FEBS Lett* **328**, 275-279.

120. Lubkowski J, Wlodawer A, Ammon HL, Copeland TD & Swain AL (1994) Structural characterization of *Pseudomonas* 7A glutaminase-asparaginase. *Biochemistry* **33**, 10257-10265.

121. Wikman LE, Krasotkina J, Kuchumova A, Sokolov NN & Papageorgiou AC (2005) Crystallization and preliminary crystallographic analysis of L-asparaginase from *Erwinia carotovora*. *Acta Crystallogr Sect F Struct Biol Cryst Commun* **61**, 407-409.

122. Papageorgiou AC, Posypanova GA, Andersson CS, Sokolov NN & Krasotkina J (2008) Structural and functional insights into *Erwinia carotovora* L-asparaginase. *FEBS J* **275**, 4306-4316.

123. Lubkowski J, Palm GJ, Gilliland GL, Derst C, Rohm KH & Wlodawer A (1996) Crystal structure and amino acid sequence of *Wolinella succinogenes* L-asparaginase. *Eur J Biochem* **241**, 201-207.

124. Derst C, Wehner A, Specht V & Rohm KH (1994) States and functions of tyrosine residues in *Escherichia coli* asparaginase II. *Eur J Biochem* **224**, 533-540.

125. Palm GJ, Lubkowski J, Derst C, Schleper S, Rohm KH & Wlodawer A (1996) A covalently bound catalytic intermediate in *Escherichia coli* asparaginase: crystal structure of a Thr-89-Val mutant. *FEBS Lett* **390**, 211-216.

126. Aung HP, Bocola M, Schleper S & Rohm KH (2000) Dynamics of a mobile loop at the active site of *Escherichia coli* asparaginase. *Biochim Biophys Acta* **1481**, 349-359.

127. Cappelletti D, Chiarelli LR, Pasquetto MV, Stivala S, Valentini G & Scotti C (2008) *Helicobacter pylori* L-asparaginase: a promising chemotherapeutic agent. *Biochem Biophys Res Commun* **377**, 1222-1226.

128. Bradford MM (1976) A rapid and sensitive method for the quantitation of microgram quantities of protein utilizing the principle of protein-dye binding. *Anal Biochem* **72**, 248-254.

129. Otwinowski Z & Minor W (1997) Processing of X-ray diffraction data collected in oscillation mode. *Method Enzymol* **276**, 307-326.

130. McCoy AJ, Grosse-Kunstleve RW, Adams PD, Winn MD, Storoni LC & Read RJ (2007) Phaser crystallographic software. *J Appl Crystallogr* **40**, 658-674.

131. Collaborative Computational Project No4 (1994) The CCP4 suite: programs for protein crystallography. *Acta Crystallogr D Biol Crystallogr* **50**, 760-763.

132. Emsley P & Cowtan K (2004) Coot: model-building tools for molecular graphics. *Acta Crystallogr D Biol Crystallogr* **60**, 2126-2132.

133. Painter J & Merritt EA (2006) Optimal description of a protein structure in terms of multiple groups undergoing TLS motion. *Acta Crystallogr D Biol Crystallogr* **62**, 439-450.

134. Painter J & Merritt EA (2006) *TLSMD* web server for the generation of multi-group TLS models. *J Appl Cryst* **39**, 109-111.

135. Murshudov GN, Vagin AA & Dodson EJ (1997) Refinement of macromolecular structures by the maximum-likelihood method. *Acta Crystallogr D Biol Crystallogr* **53**, 240-255.

136. Dixon DP, McEwen AG, Lapthorn AJ & Edwards R (2003) Forced evolution of a herbicide detoxifying glutathione transferase. *J Biol Chem* **278**, 23930-23935.

137. Sheldrick GM (2008) A short history of SHELX. *Acta Crystallogr A* **64**, 112-122.

138. Schuttelkopf AW & van Aalten DM (2004) PRODRG: a tool for high-throughput crystallography of protein-ligand complexes. *Acta Crystallogr D Biol Crystallogr* **60**, 1355-1363.

139. Lovell SC, Davis IW, Arendall WB, 3rd, de Bakker PI, Word JM, Prisant MG, Richardson JS & Richardson DC (2003) Structure validation by Calpha geometry: phi,psi and Cbeta deviation. *Proteins* **50**, 437-450.

140. Laskowski RA, MacArthur MW, Moss DS & Thornton JM (1993) PROCHECK: A program to check the stereochemical quality of protein structures. *J Appl Crystallogr* **26**, 283-291.

141. Thompson JD, Higgins DG & Gibson TJ (1994) CLUSTAL W: improving the sensitivity of progressive multiple sequence alignment through sequence weighting, position-specific gap penalties and weight matrix choice. *Nucleic Acids Res* **22**, 4673-4680.

142. Kabsch W & Sander C (1983) Dictionary of protein secondary structure: pattern recognition of hydrogen-bonded and geometrical features. *Biopolymers* **22**, 2577-2637.

143. Gouet P, Robert X & Courcelle E (2003) ESPript/ENDscript: Extracting and rendering sequence and 3D information from atomic structures of proteins. *Nucleic Acids Res* **31**, 3320-3323.

144. Prade L, Huber R & Bieseler B (1998) Structures of herbicides in complex with their detoxifying enzyme glutathione S-transferase - explanations for the selectivity of the enzyme in plants. *Structure* **6**, 1445-1452.

145. Axarli I, Dhavala P, Papageorgiou AC & Labrou NE (2009) Crystal structure of *Glycine max* glutathione transferase in complex with glutathione: investigation of the mechanism operating by the Tau class glutathione transferases. *Biochem J* **422**, 247-256.

146. Matthews BW (1968) Solvent content of protein crystals. *J Mol Biol* **33**, 491-497.

147. Kantardjieff KA & Rupp B (2003) Matthews coefficient probabilities: Improved estimates for unit cell contents of proteins, DNA, and protein-nucleic acid complex crystals. *Protein Sci* **12**, 1865-1871.

148. Lubkowski J, Wlodawer A, Housset D, Weber IT, Ammon HL, Murphy KC & Swain AL (1994) Refined crystal structure of *Acinetobacter glutaminasificans* glutaminase-asparaginase. *Acta Crystallogr D Biol Crystallogr* **50**, 826-832.

149. Kravchenko OV, Kislitsin YA, Popov AN, Nikonov SV & Kuranova IP (2008) Three-dimensional structures of L-asparaginase from *Erwinia carotovora* complexed with aspartate and glutamate. *Acta Crystallogr D Biol Crystallogr* **64**, 248-256.

150. Dhavala P & Papageorgiou AC (2009) Structure of *Helicobacter pylori* L-asparaginase at 1.4 A resolution. *Acta Crystallogr D Biol Crystallogr* **65**, 1253-1261.

151. Burmeister WP (2000) Structural changes in a cryo-cooled protein crystal owing to radiation damage. *Acta Crystallogr D Biol Crystallogr* **56**, 328-341.